Université de Neuchâtel
Institut de Microtechnique

Holographic Optical Scanning Elements

Thèse

Présentée à la Faculté des sciences
pour obtenir le grade de docteur ès sciences

par

Hans Peter Herzig

IMPRIMATUR POUR LA THÈSE

Holographic Optical Scanning Elements

de Monsieur Hans Peter Herzig

UNIVERSITÉ DE NEUCHATEL

FACULTÉ DES SCIENCES

La Faculté des sciences de l'Université de Neuchâtel,
sur le rapport des membres du jury,

Messieurs R. Dändliker, P. Martinoli,
H. Buczek (Neuchâtel) et A. Friesem (Rehovot)

autorise l'impression de la présente thèse.

Neuchâtel, le 14 août 1987

Le doyen:

François Sigrist

ABSTRACT

A new analytical method for designing holographic optical elements (HOEs) in focussing laser scanner applications is presented. These elements are designed to have minimum aberrations and optimum scan line definition. The required aspherical wave for recording an efficient volume holographic scanner is derived from a computer generated hologram (CGH). Moreover, the CGH corrects also the aberrations that arise from change of wavelengths between recording and readout of the scanning element. Such a change is imposed by the discrepancy between the spectral sensitivity of the photosensitive recording materials (typically <520 nm) and the wavelength of the readout sources (>630 nm, He-Ne, AlGaAs).

It is shown that the analytical method can be easily applied to specific scan problems using second order approximation for the incident and the outgoing beams. The optimum design of a holographic disk scanner, which generates a straight line in space by a circular motion, is emphasized. The results reveal that the focussed spots along the straight line always contain astigmatism. However, by accepting small deviations from the straight line, the astigmatism can be eliminated and the quality of the focal spot can be improved. For example, we obtained spot diameters (at half intensity) of less than 85 μm for a maximum scan line deviation of ±8 μm and less than 60 μm for a maximum scan line deviation of ±30 μm, at any position within the scan length of ±105 mm and an image plane distance of 300 mm.

By extending the method to higher order approximations, it was found that aberrations perpendicular to the scan line can be reduced with appropriate corrections of the hologram phase function. However, astigmatism and other higher order aberrations, especially along the scan line cannot be removed completely.

CONTENTS

1. INTRODUCTION

Holographic optical elements (HOEs) can serve as the deflecting as well as the focussing element in laser scanners. They have been incorporated into supermarket point of sale systems [1,2], laser-beam printers [3] and are expected to be useful in a wide range of future applications [4,5]. The review article by G. T. Sincerbox [6] is a good general introduction in holographic scanners. In the following we shall briefly present the principles of holographic laser scanners, describe some basic configurations and recent developments, and then give a summary of our own work.

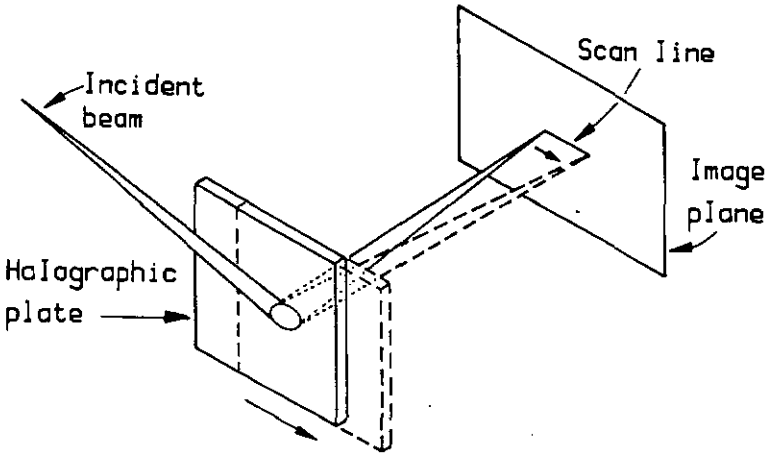

Fig.1.1. Principle of holographic laser scanners.

A focussing HOE (holographic lens) can be realized by recording the interference pattern of two coherent spherical waves, a reference wave and an object wave, in a photosensitive holographic emulsion. By illuminating the HOE with a readout wave (e.g. a replica of the reference wave), the object wave is reconstructed and produces a focused beam. As the HOE is translated (Fig.1.1), the image point moves also and generates a scan line parallel to the mechanical motion. This is a rather simplistic view of holographic deflection and is only intended to present the basic concept.

Rather than translating the hologram, the configurations with rotating elements are of greater practical interest. One such configuration, shown in Fig.1.2, is the disk scanner, using a flat substrate and collimated illumination, proposed in 1967 by Cindrich [7]. It has aberration-free reconstruction when the reference beam is either parallel to the rotation axis, or originates from a point on the rotation axis. Another configuration with a rotating element, shown in Fig.1.3, is the drum configuration scanner, demonstrated in 1975 by Pole and Wollenman [8], where the hologram is on a cylindrical surface. The point of convergence of the outgoing wave remains in a plane orthogonal to the rotation axis, thereby simplifying the problem of getting a straight scan line. There exist many other similar configurations with spherical concave or convex surfaces (Beiser, et al. [9], in 1973) and others, that work in transmission or reflection. Because of the rotational symmetry of these scanner types, the image point describes a circle or an arc. For some applications, such as point of sale systems, a curved scan line can be accepted. However, for other applications, such as laser printers, the straightness of the scan line and the spot quality are far more critical.

Disk-like devices are relatively easy to manufacture. As a result, substantial work has been conducted for approximating a straight-line image by disk configuration scanners. A possible solution for designing a straight-line scanner is to employ an auxiliary optical element. For example, the design proposed 1977 by Ih [10] uses a spherical deflector, whereas the design proposed 1981 by Kramer [11], uses an imaging lens. Of course, it would be advantageous to avoid additional elements, if possible. This could be done by exploiting the full potential of HOEs, that are recorded with aspherical wavefronts. Indeed, having aspherical waves, it is possible to design almost any special HOEs. Aspherical wavefronts can be formed by properly combining several spherical waves [12], by exploiting specially designed optical systems [13], by using computer generated holograms (HOEs) [14], and so on. A step in this direction was made in 1976 by Bryngdahl and Lee [15], using CGHs for holographic scanners.

Another serious problem in holographic laser scanning that must be solved, is the wavelength shift between recording and reconstruction, which causes strong aberations. The wavelength shift is imposed by the discrepancy between the spectral sensitivity of the photosensitive materials (typically < 520 nm , for high efficiency holographic materials) and the wavelength of the readout sources (> 630 nm, for He-Ne or AlGaAs lasers).

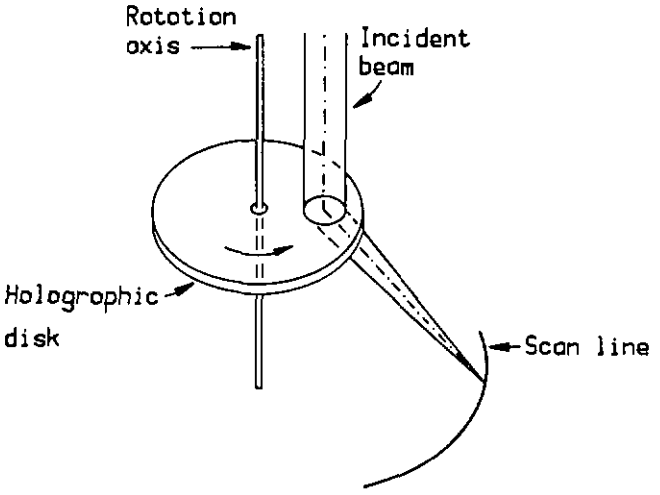

Fig.1.2. Disk configuration scanner.

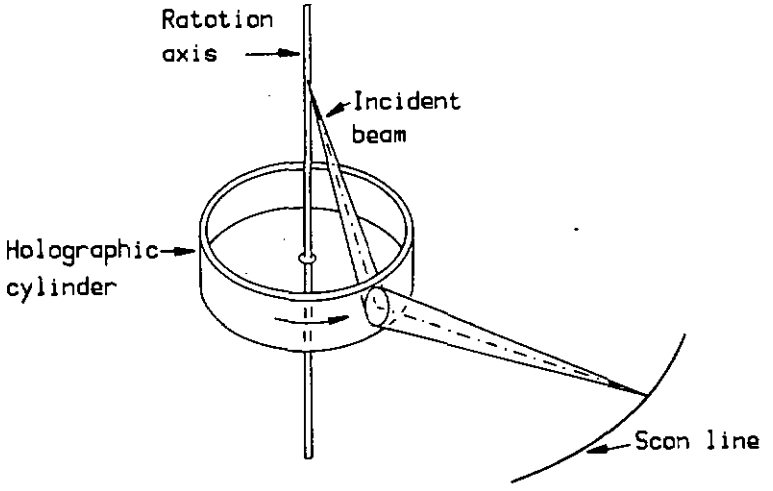

Fig.1.3. Drum configuration scanner.

No matter how the hologram is produced, it is possible to represent the hologram structure by a phase function $\Phi(x,y)$. To find the ideal phase function Φ for a special scan configuration is, in general, a complex problem. Possible solutions involve numerical optimum design methods, similar to the ones commonly used for optimizing lens systems in classical optics. A merit function has to be defined, which describes the scan quality, and by changing the wavefront parameters this merit function is minimized [16,17]. Such methods work well to find a local minimum for the specified configuration, but do not yield informations about a general solution, nor about the influence of the different parameters. An alternative method to determine the hologram phase function Φ analytically, first introduced in 1983 by Winick and Fienup, is based on minimizing of the mean-squared wavefront [18,19]. This method, however, was never applied for designing holographic scanners.

This thesis presents a new analytical method [20,21], which is differential rather than integral, for determining the phase function necessary to solve particular scan problems. With this method it is possible to determine the basic behaviours of scanners and the results are not limited to a special choice of phase functions Φ for describing the hologram. Furthermore, since the results are more explicit, it is possible to determine the influence of the geometrical parameters and the scan line geometry on the spot quality, thereby yielding improved scanner configurations.

In the remainder of this thesis, chapter 2 introduces the basic principles and develops the generalized scan equation. The application of the analytical method to specific scan configurations (3.1 Linear translation scanners, 3.2 Disk configuration scanners, 3.3 Drum configuration scanners) is easily possible using second order approximation for the incident and the outgoing beams. The emphasis is on the optimum design of holographic disk scanners (section 3.2), which generate a straight line in space by a circular motion. In the experimental part (chapter 4) disk scanners are realized with a wavelength shift between recording (514 nm) and reconstruction (633 nm). The scan quality (line straightness and spot quality) are compared with the theoretical results. To determine the degree of freedom for higher order corrections, the theory has been extended up to fourth order (chapter 5). The quality of the analytical solutions is examined by geometrical ray tracing.

2. THEORY

2.1 Basic equations

A laser beam is deflected and focussed by a holographic optical element (HOE), which can be described by a phase function $\Phi(x,y)$. While displacing the HOE, the incident beam moves along a line $\mathbf{x}(s)$ in the hologram plane and the image point describes another line $\mathbf{y}(t)$ in space (Fig.2.1). In order to generate a particular line $\mathbf{y}(t)$ in space, it is necessary to determine the appropriate phase function $\Phi(x,y)$.

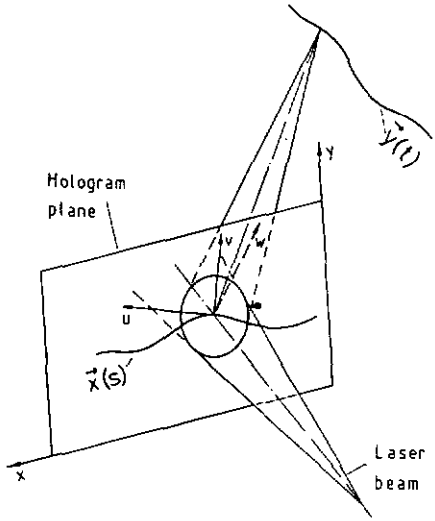

Fig.2.1. General scan configuration. The hologram moves along a line x(s) in the hologram plane and the image point describes another line y(t) in space.

A local coordinate system u,v,w is introdueed, so that the w-axis is normal to the hologram plane. During the scan motion, this coordinate system is fixed in spaee, as are the incident laser beam and the generated line $\mathbf{y}(t)$. The origin of the system u,v,w is at the center of the incident laser beam in the hologram plane and on the line $\mathbf{x}(s)$. For each position t on the line $\mathbf{y}(t)$ the local phase function $\Psi(u,v,t)$ in the hologram plane can be written as

$$\Psi(u,v,t) = \Phi_p(u,v,t) - \Phi_r(u,v). \qquad (2.1)$$

where Φ_p describes the phase of the outgoing wave, focussed on the line $\mathbf{y}(t)$, and Φ_r represents the phase of the incident reconstructing laser beam.

The coordinate system x,y is fixed in the hologram plane and moves with it during the scan. The incident laser beam moves in the hologram plane on the line $\mathbf{x}(s)$. At each point on $\mathbf{x}(s)$, characterized by the parameter s, the incident beam reconstructs a point on the line $\mathbf{y}(t)$, characterized by the parameter t. Therefore, within the pupil of the laser beam centered at the point s, the phase function $\Phi(x,y)$ of the hologram should be identical to the phase function $\Psi(u,v,t)$ given in Eq.(2.1). In general, this condition cannot be fulfilled rigorously for all points of a continuous scan. To get at least a local match of the two phase functions Φ and Ψ, they are both expanded in Taylor series about the point $\mathbf{x}(s)$, which corresponds to the origin of the u,v- coordinate system, viz.

$$\Phi(u,v,s) = \Phi(\mathbf{x}(s)) + \frac{\partial\Phi}{\partial u_i}\Big|_s u_i + \frac{1}{2}\frac{\partial^2\Phi}{\partial u_i \partial u_j}\Big|_s u_i u_j + \ldots \qquad i,j = 1,2, \tag{2.2}$$

$$\Psi(u,v,t) = \Psi(0,0,t) + \frac{\partial\Psi}{\partial u_i}\Big|_t u_i + \frac{1}{2}\frac{\partial^2\Psi}{\partial u_i \partial u_j}\Big|_t u_i u_j + \ldots \tag{2.3}$$

Here and in the following, two notations are used for the components of the spatial vectors, namely $\mathbf{u} = (u,v,w) = (u_1,u_2,u_3)$ and $\mathbf{x} = (x,y,z) = (x_1,x_2,x_3)$.

We require now, that the two series are equal up to second order, where the first order derivatives determine the direction and the second order derivatives the curvature of the outgoing wave. This yields the following six conditions:

$$\Phi(\mathbf{x}(s)) = \Psi(0,0,t). \tag{2.4}$$

$$\frac{\partial\Phi}{\partial u_i}\Big|_s = \frac{\partial\Psi}{\partial u_i}\Big|_t \equiv h_i(t). \qquad i,j = 1,2, \tag{2.5}$$

$$\frac{\partial^2\Phi}{\partial u_i \partial u_j}\Big|_s = \frac{\partial^2\Psi}{\partial u_i \partial u_j}\Big|_t \equiv h_{ij}(t). \tag{2.6}$$

To find the phase function $\Phi(x,y)$, the relations between the derivatives in the two coordinate systems x,y and u,v have to be established. These relations depend on the geometry of the particular scan problem, and can be formally

expressed with the aid of five functions f_i and f_{ij}, namely

$$\frac{\partial \Phi}{\partial x_i}\Big|_S = f_i\left(\frac{\partial \Phi}{\partial u_k}\Big|_S\right). \tag{2.7}$$

$$\frac{\partial^2 \Phi}{\partial x_i \partial x_j}\Big|_S = f_{ij}\left(\frac{\partial \Phi}{\partial u_k}\Big|_S, \frac{\partial^2 \Phi}{\partial u_l \partial u_m}\Big|_S\right). \tag{2.8}$$

Introducing Eqs.(2.5) and (2.6) in Eqs.(2.7) and (2.8), yields

$$\frac{\partial \Phi}{\partial x_i}\Big|_S = f_i(h_k(t)) \equiv g_i(t). \tag{2.9}$$

$$\frac{\partial^2 \Phi}{\partial x_i \partial x_j}\Big|_S = f_{ij}(h_k(t), h_{lm}(t)) \equiv g_{ij}(t). \tag{2.10}$$

The five relations of Eqs.(2.9) and (2.10) have to be fulfilled simultaneously by one and the same phase function $\Phi(x,y)$ along the line $\mathbf{x}(s)$. Thus, Eqs.(2.9) and (2.10) determine all possible solutions, for which the outgoing wave has the desired direction and the desired curvature.

For the solution of a particular scan problem, it is necessary to determine first the functions $h_i(t)$ and $h_{ij}(t)$. They are, following Eqs.(2.5) and (2.6), equal to the first and second derivatives of the local phase function $\Psi(u,v,t)$ [Eq.(2.1)] required at the origin (u=v=0) to focus the outgoing wave into the point t along the line $\mathbf{y}(t)$. In addition, one has to establish for the particular scan geometry the relations (f_i, f_{ij}) between the derivatives in the two coordinate systems x,y and u,v [Eqs.(2.7) and (2.8)] to get finally the Eqs.(2.9) and (2.10) in explicit form. The value of the phase function $\Phi(x,y)$ along $\mathbf{x}(s)$ [Eq.(2.4)] follows by integration of Eq.(2.9). In section 2.3 it will be shown that, in general, an astigmatic solution can be found by this way for any particular scan problem. Later, in chapter 5, higher order aberrations will also be considered.

2.2 Scan equation

As mentioned above, Eqs.(2.9) and (2.10) describe all possible solutions. Of special interest is the relation between the two scan parameters s and t. If the incident laser beam falls onto the hologram with the beam center at a point s on $\mathbf{x}(s)$, it will reconstruct a well defined point t on $\mathbf{y}(t)$; thus, t is related to s. To find the scan function t(s), it is necessary to follow the evolution of the first and second derivatives of $\Phi(x,y)$ along the line $\mathbf{x}(s)$. They are given by

$$\frac{d\Phi}{ds} = \frac{\partial\Phi}{\partial x}\frac{dx}{ds} + \frac{\partial\Phi}{\partial y}\frac{dy}{ds} . \tag{2.11}$$

$$\begin{aligned}\frac{d^2\Phi}{ds^2} = {} & \frac{\partial^2\Phi}{\partial x^2}\left(\frac{dx}{ds}\right)^2 + \frac{\partial^2\Phi}{\partial y\partial x}\frac{dy}{ds}\frac{dx}{ds} + \frac{\partial\Phi}{\partial x}\frac{d^2x}{ds^2} \\ & + \frac{\partial^2\Phi}{\partial y^2}\left(\frac{dy}{ds}\right)^2 + \frac{\partial^2\Phi}{\partial x\partial y}\frac{dx}{ds}\frac{dy}{ds} + \frac{\partial\Phi}{\partial y}\frac{d^2y}{ds^2} .\end{aligned} \tag{2.12}$$

Using Eqs.(2.9) and (2.10) yields the following conditions for the derivatives along the line $\mathbf{x}(s)$:

$$\left.\frac{d\Phi}{ds}\right|_s = g_1(t)\frac{dx}{ds} + g_2(t)\frac{dy}{ds} . \tag{2.13}$$

$$\begin{aligned}\left.\frac{d^2\Phi}{ds^2}\right|_s = {} & g_{11}(t)\left(\frac{dx}{ds}\right)^2 + g_{21}(t)\frac{dy}{ds}\frac{dx}{ds} + g_1(t)\frac{d^2x}{ds^2} \\ & + g_{22}(t)\left(\frac{dy}{ds}\right)^2 + g_{12}(t)\frac{dx}{ds}\frac{dy}{ds} + g_2(t)\frac{d^2y}{ds^2} .\end{aligned} \tag{2.14}$$

Equations (2.13) and (2.14) are derivatives of one and the same phase function, so they are not independent. The change of the first derivative along s must be equal to the second derivative, which means that

$$\frac{d}{ds}\left(\left.\frac{d\Phi}{ds}\right|_s\right) = \left.\frac{d^2\Phi}{ds^2}\right|_s . \tag{2.15}$$

Introducing Eqs.(2.13) and (2.14) into Eq.(2.15) and using $g_{12} = g_{21}$ yields the

scan cquation

$$\frac{dt}{ds}\left(\frac{dg_1}{dt}\frac{dx}{ds} + \frac{dg_2}{dt}\frac{dy}{ds}\right) - g_{11}\left(\frac{dx}{ds}\right)^2 - g_{22}\left(\frac{dy}{ds}\right)^2 - 2g_{12}\frac{dx}{ds}\frac{dy}{ds} = 0, \qquad (2.16)$$

which is a differential equation for the scan function t(s). Thc function t(s) is obtained by integrating Eq.(2.16) and is therefore completely determined by thc gcometry of the scan problem. As a consequence, the scan motion on the line **x**(s), necessary to perform a certain scan length on the line **y**(t), is given by t(s) and cannot be chosen freely.

2.3 Holography with astigmatic pencils of rays

When limiting the Taylor expansion to only two orders, the outgoing wave can be described as an astigmatic pencil of rays (Fig.2.2). It is characterized by the direction of propagation, given by the wavevector **k**, and the two focal lines at the distances ρ_1 and ρ_2, respectively. This corresponds to a second order, approximation, where astigmatic waves can occur [22]. In this approximation, the optical phase is found to be

$$\phi_P(\mathbf{X}) = \phi_{P0} + \left(\frac{\partial\phi_P}{\partial X_i}\right) X_i + \frac{1}{2}\left(\frac{\partial^2\phi_P}{\partial X_i \partial X_j}\right) X_i X_j . \qquad i,j = 1,2,3. \qquad (2.17)$$

The Z-axis is chosen to be parallel to the direction of propagation, so that $(\partial\phi_P/\partial X) = 0$, $(\partial\phi_P/\partial Y) = 0$ and $(\partial\phi_P/\partial Z) = k$, where $k = 2\pi/\lambda$ is the wavenumber. The curvature of the wavefront is then described by the three-dimensional, symmetric tensor with the components $\kappa_{XX} \equiv a$, $\kappa_{YY} \equiv b$, and $\kappa_{XY} = \kappa_{YX} \equiv c$, as

$$\kappa_{ij} = \frac{\partial^2\phi_P}{\partial X_i \partial X_j} \equiv k \begin{bmatrix} a & c & 0 \\ c & b & 0 \\ 0 & 0 & 0 \end{bmatrix} . \qquad (2.18)$$

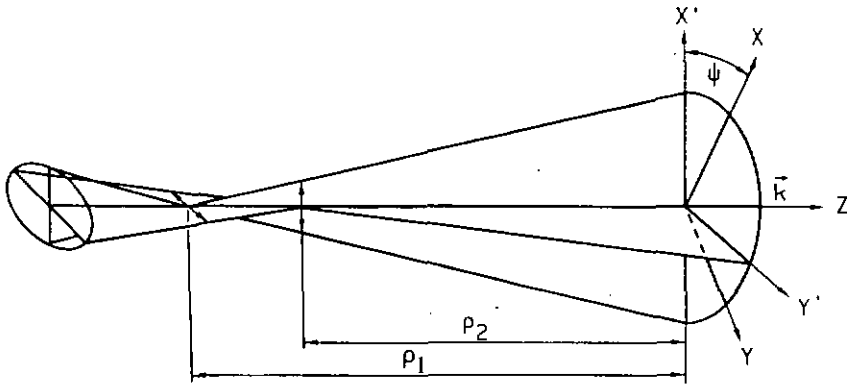

Fig.2.2. Astigmatic pencil of rays.

Diagonalization of the tensor κ_{ij} yields the principal direction ψ and the principal radii of curvature ρ_1 and ρ_2 (Fig.2.2).

$$\tan 2\psi = 2\,c/(a - b). \tag{2.19}$$

$$1/\rho_1,\rho_2 = (1/2)(a + b) \pm [(1/2)(a - b)\cos 2\psi + c \sin 2\psi]. \tag{2.20}$$

From Eq.(2.20) the mean radius of curvature ρ_m, i.e. the distance to the circle of least confusion, and the astigmatism A are deduced as

$$1/\rho_m = (1/2)(1/\rho_1 + 1/\rho_2) = (1/2)(a + b), \tag{2.21}$$

$$A = (1/2)(1/\rho_1 - 1/\rho_2) = (1/2)(a - b)\cos 2\psi + c \sin 2\psi. \tag{2.22}$$

Using Eq.(2.19) the amount of astigmatism can be written differently as

$$A^2 = (a - b)^2/4 + c^2\,. \tag{2.23}$$

The phase in the hologram plane $\Psi(u,v)$ is essentially governed by the condition of phase matching, which reads

$$\Psi(\mathbf{u}_H) = \Phi_p(\mathbf{u}_H) - \Phi_r(\mathbf{u}_H), \tag{2.24}$$

where r means the reconstructing reference and P the reconstructed astigmatic wave front. Therefore the phase distributions for each pencil of rays in the hologram plane has to be calculated first. The geometrical relation between the hologram plane and the reconstructed pencil of rays is sketched in Fig.2.3. The direction of propagation is given by two angles α and β, so that the components of the wavevector $\mathbf{k}$ are

$$k_u = k \sin\beta, \quad k_v = k \sin\alpha \cos\beta, \quad k_w = k \cos\alpha \cos\beta, \tag{2.25}$$

with $-\pi/2 < \alpha < \pi/2$, $-\pi/2 < \beta < \pi/2$ and $k = 2\pi/\lambda$.

Note that the wavevector $\mathbf{k}$ is assumed to point in the positive direction of the w-axis. This restriction is necessary to distinguish between divergent ($\rho > 0$) and convergent ($\rho < 0$) waves.

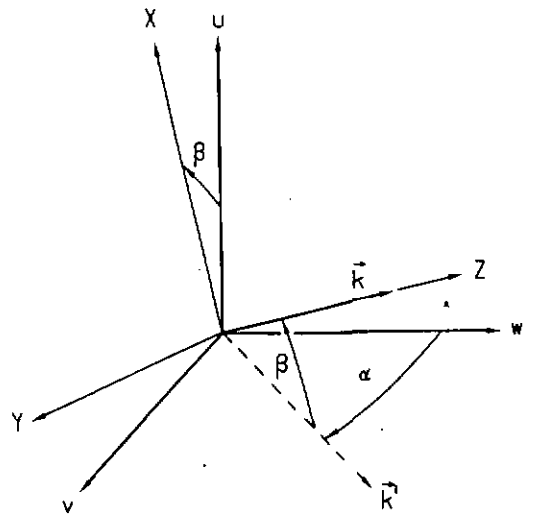

Fig.2.3. Geometrical relation of the hologram plane (u,v) and a pencil of rays. The wavevector k is parallel to the Z-axis. k' is the projection of k onto the plane (v,w).

The transformation from the (X,Y,Z) to the (u,v,w) coordinates is performed by two subsequent rotations. The first is around the Y-axis by the angle β and the second is then around the u-axis by the angle α. The corresponding transformation matrix R is found to be

$$R = \begin{bmatrix} \cos\beta & 0 & \sin\beta \\ -\sin\alpha\sin\beta & \cos\alpha & \sin\alpha\cos\beta \\ -\cos\alpha\sin\beta & -\sin\alpha & \cos\alpha\cos\beta \end{bmatrix} . \qquad (2.26)$$

Furthermore, the direction of the outgoing wave and the tensor of curvature have to be projected onto the hologram plane. This projection tensor P becomes in (u,v,w) coordinates

$$P = \begin{bmatrix} 1 & 0 & 0 \\ 0 & 1 & 0 \\ 0 & 0 & 0 \end{bmatrix} \qquad (2.27)$$

For the direction $\mathbf{m}_p$ of the outgoing wave and the tensor of curvature χ_p in the hologram plane follows then

$$\mathbf{m}_p = P\,R\,\mathbf{k} = k\,(\sin\beta,\ \sin\alpha\cos\beta), \tag{2.28}$$

$$\chi_p = P\,R\,\kappa\,R^{-1}\,P = \tag{2.29}$$

$$k\begin{bmatrix} a\cos^2\beta & -a\sin\alpha\sin\beta\cos\beta + c\cos\alpha\cos\beta \\ -a\sin\alpha\sin\beta\cos\beta + c\cos\alpha\cos\beta & a\sin^2\alpha\sin^2\beta - 2c\sin\alpha\cos\alpha\sin\beta + b\cos^2\alpha \end{bmatrix},$$

where $\mathbf{k}$ and κ are given in the (X,Y,Z) system and $\mathbf{m}_p$ and χ_p in the hologram plane (u,v).

During the scan motion the direction of propagation $\mathbf{k}$ and the curvature κ of the outgoing wave will change with the scan parameter t (Fig.2.1). This means that both Eqs.(2.28) and (2.29) are functions of t through $\alpha(t)$, $\beta(t)$, $a(t)$, $b(t)$ and $c(t)$. To generate a particular scan line $\mathbf{y}(t)$ in space, these functions have to be established from geometrical considerations. For a straight line $\mathbf{y}(t)$ in space, the direction of the outgoing wave remains in a plane, which can be assumed to contain the u-axis of the hologram plane (Fig.2.3). In this case, α is constant during the scan (α = const).

The incident beam (Φ_r) can be treated in the same second order approximation. It keeps its position in space during the scan motion. The direction of propagation is now characterized by the two angles γ and δ, where γ corresponds to α and δ to β in Fig.2.3. We assume that the incident wave is spherical with radius ρ, which means that $a = b = 1/\rho$ and $c = 0$. Thus the direction $\mathbf{m}_r$ and the tensor of curvature χ_r of the incident wave in the hologram plane become

$$\mathbf{m}_r = k\,(\sin\delta,\ \sin\gamma\cos\delta), \tag{2.30}$$

$$\chi_r = (k/\rho)\begin{bmatrix} \cos^2\delta & -\sin\gamma\sin\delta\cos\delta \\ -\sin\gamma\sin\delta\cos\delta & \sin^2\gamma\sin^2\delta + \cos^2\gamma \end{bmatrix}. \tag{2.31}$$

Using the relations of Eqs.(2.28) to (2.31), the local phase distribution in the

hologram plane can be calculated up to second order from

$$\Psi(\mathbf{u}_H,t) = \Psi_o + \mathbf{m}^T \mathbf{u}_H + (1/2)(\mathbf{u}_H)^T \chi \mathbf{u}_H , \tag{2.32}$$

where $\mathbf{m}$ and χ are obtained from the condition of phase matching in Eq.(2.24), to yield

$$\mathbf{m}(\mathbf{u}_H,t) = (\frac{\partial\Psi}{\partial u_i}|_t) = \mathbf{m}_p(\mathbf{u}_H,t) - \mathbf{m}_r(\mathbf{u}_H) = h_i(t). \tag{2.33}$$

$$\chi(\mathbf{u}_H,t) = (\frac{\partial^2\Psi}{\partial u_i \partial u_j}|_t) = \chi_p(\mathbf{u}_H,t) - \chi_r(\mathbf{u}_H) = h_{ij}(t). \tag{2.34}$$

Equations (2.33) and (2.34) describe the first and second derivatives of the local phase function $\Psi(u,v,t)$, i.e. $h_i(t)$ and $h_{ij}(t)$ in Eqs.(2.5) and (2.6). In order to proceed and determine the hologram phase function $\Phi(x,y)$, the relations between the derivatives in the two coordinate systems x,y and u,v have to be established. They depend on the geometry of the scanning configuration, and, in particular, on the motion $\mathbf{x}(s)$ of the incident beam in the plane of the HOE scanner. This will be done for three different scanning geometries in chapter 3.

3. SCANNING CONFIGURATIONS

In this chapter three different scanning configurations are analyzed, namely linear translation scanners, disk configuration scanners and drum configuration scanners.

3.1 Linear translation scanners

We shall first explore the linear translation scanners, where the hologram moves along a straight line $\mathbf{x}(s)$ and the outgoing wave generates also a straight line $\mathbf{y}(t)$ in space, as shown in Fig.3.1. The linear motion of the hologram is assumed to be parallel to the generated line $\mathbf{y}(t)$ and parallel to the x-axis, which is therefore also parallel to the u-axis. In this situation, it is convenient to use x as the scan parameter s in the hologram plane (x = s) and the deflection angle β as the scan parameter t in space (β = t). The derivatives of Φ in the two coordinate systems x,y and u,v [Eqs.(2.7) and (2.8)] are then simply related by

$$\frac{\partial \Phi}{\partial x_i} = \frac{\partial \Phi}{\partial u_i}, \qquad \frac{\partial^2 \Phi}{\partial x_i \partial x_j} = \frac{\partial^2 \Phi}{\partial u_i \partial u_j}, \qquad i,j = 1,2. \tag{3.1}$$

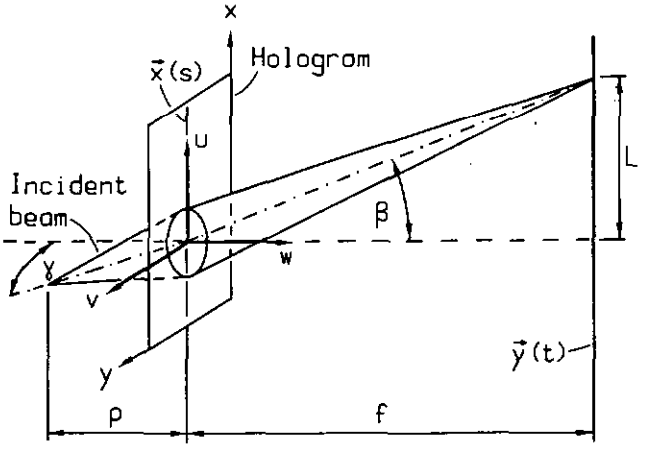

Fig.3.1. Linear motion x(s) of the hologram to generate a straight line y(t).

Introducing these relations into Eqs.(2.9) and (2.10), yields for the derivatives of $\Phi(x,y)$ on the scan line $\mathbf{x}(s) = (x, y=0)$

$$\frac{\partial \Phi}{\partial x_i}\Big|_{y=0} \equiv g_i(\beta) = h_i(\beta), \qquad \frac{\partial^2 \Phi}{\partial x_i \partial x_j}\Big|_{y=0} \equiv g_{ij}(\beta) = h_{ij}(\beta), \tag{3.2}$$

where h_i and h_{ij} are given by the local phase $\Psi(u,v,\beta)$ required for the desired outgoing wave [Eqs.(2.5) and (2.6)].

Using second order approximation, the functions $h_i(\beta)$ and $h_{ij}(\beta)$ can be obtained with the help of Eqs.(2.33) and (2.34). For the scan geometry shown in Fig.3.1, with $\alpha \neq 0$ and $\delta = 0$, follows

$$h_1 = k \sin\beta, \quad h_2 = k (\sin\alpha \cos\beta - \sin\gamma), \tag{3.3}$$

$$h_{11} = k (a \cos^2\beta - 1/\rho), \tag{3.4a}$$

$$h_{12} = h_{21} = k (c \cos\alpha \cos\beta - a \sin\alpha \sin\beta \cos\beta), \tag{3.4b}$$

$$h_{22} = k (a \sin^2\alpha \sin^2\beta - 2 c \sin\alpha \cos\alpha \sin\beta + b \cos^2\alpha - \cos^2\gamma/\rho). \tag{3.4c}$$

To get the scan equation [cf. Eqs.(2.15) and (2.16)] and the phase function $\Phi(x,y)$, it is necessary to follow the development of $\Phi(x,y)$ along the scan line $\mathbf{x}(s) = (x, y=0)$. Perpendicular to the scan line, i.e. in the y-direction, a second order (parabolic) approximation of $\Phi(x,y)$ will be sufficient to satisfy Eqs.(3.2). Therefore, the phase function may be written as

$$\Phi(x,y) = k [a_0(x) + a_1(x)\, y + (1/2)\, a_2(x)\, y^2]. \tag{3.5}$$

Applying Eqs.(3.2), (3.3) and (3.4) to Eq.(3.5), yields finally

$$a_0' = \sin\beta, \quad a_0'' = a \cos^2\beta - 1/\rho, \tag{3.6}$$

$$a_1 = \sin\alpha \cos\beta - \sin\gamma, \quad a_1' = c \cos\alpha \cos\beta - a \sin\alpha \sin\beta \cos\beta, \tag{3.7}$$

$$a_2 = a \sin^2\alpha \sin^2\beta - 2 c \sin\alpha \cos\alpha \sin\beta + b \cos^2\alpha - \cos^2\gamma/\rho, \tag{3.8}$$

with ' = d/dx and " = d^2/dx^2.

An ideally focussed (spherical) outgoing wave requires that a = b = - cosβ/f and c = 0, where f is the distance between the hologram and the image plane [Fig.3.1].

Since the relation a_0" = d(a_0')/dx has to be fulfilled, Eqs.(3.6) yield the scan equation

$$d\beta/dx - a(\beta)\cos\beta + 1/(\rho\cos\beta) = 0, \qquad (3.9)$$

where a(β) = - cosβ/f. Equation (3.9) determines the relation β(x) between the scan angle β and the displacement x of the hologram.

Similar to Eq.(3.9), it is necessary to fulfill $a_1' = da_1/dx$, which yields from Eqs.(3.7)

$$d\beta/dx - a(\beta)\cos\beta + c(\beta)/(\tan\alpha\tan\beta) = 0. \qquad (3.10)$$

Since the scan equation (3.9) and Eq.(3.10) have to be satisfied simultaneously, then for c(β) we obtain the condition

$$c(\beta) = \tan\alpha\sin\beta/(\rho\cos^2\beta). \qquad (3.11)$$

As can be seen from Eq.(2.23), c essentially determines the astigmatism A of the outgoing wave. It becomes minimal (|A| = |c|) for a = b. This condition can be satisfied by choosing a_2 from Eq.(3.8) accordingly. As a consequence, there remains an astigmatism |A| = |c|, given by Eq.(3.11), with the principal direction ψ = 45 deg [Eq.(2.19)]. The astigmatism is equal to zero for β = 0, but it is not possible to maintain A equal to zero for all scan angles β, unless the incident wave is plane (ρ = ∞) or the scan plane is perpendicular to the hologram (α = 0).

In summary, it is possible to find a well defined phase function Φ(x,y) [Eq.(3.5)] for the hologram, which produces within second order approximation an ideally focussed (spherical) wave on a straight line in space.

For a better understanding of the scan equation, it is convenient to replace the angle β by the scan length $L = f \tan\beta$ in the image plane (Fig.3.1), so that Eq.(3,9) becomes

$$dL/dx = - [1 + f/(\rho \cos^3\beta)]. \qquad (3.12)$$

The right hand side of Eq.(3.12) is the differential magnification M of the scan, namely the ratio between the movement dL of the focus on the line $\mathbf{y}(t)$ and the displacement dx of the hologram. In the case of a plane incident wave ($\rho = \infty$), one obtains $M = 1$, which means that the displacement of the hologram is equal to the scan length. If the incident wave is divergent ($\rho > 0$), then $M > 1$ and the displacement of the hologram becomes smaller than the scan length.

To get more informations, including higher order aberrations, of these second order solutions, we have applied geometrical ray tracing (Appendix) to the holograms described by Eq.(3.5). The calculations have been made for a distance from scan line to hologram of $f = 300$ mm, a divergent incident beam with $\rho = 50$ mm and a diameter $D = 5$ mm of the beam in the hologram plane (Fig.3.1). To avoid astigmatism, the inclination of the scan plane was chosen to be $\alpha = 0$ [Eq.(3.11)]. Figures 3.2 show the spot diagrams for three hologram positions x with the corresponding scan lengths $L = 0$, 67.9 and 105 mm. The inclination of the incident wave is $\gamma = 0$ deg in Fig.3.2(a) and $\gamma = - 10$ deg in Fig.3.2(b). The second case shows strong higher order aberrations in the y-direction, which are caused by the inclination of the incident beam. These aberrations, perpendicular to the scan line $\mathbf{x}(s)$, can be corrected by introducing adequate higher order terms $a_i(x)$ in the phase [Eq.(3.5)], whereas in the direction of the scan line (x-direction), the aberrations are completely determined by the solution of the scan equation (3.9).

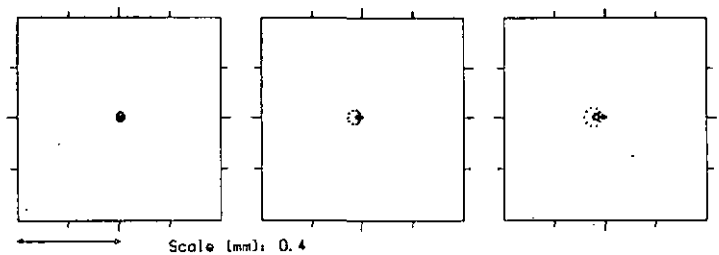

(a)

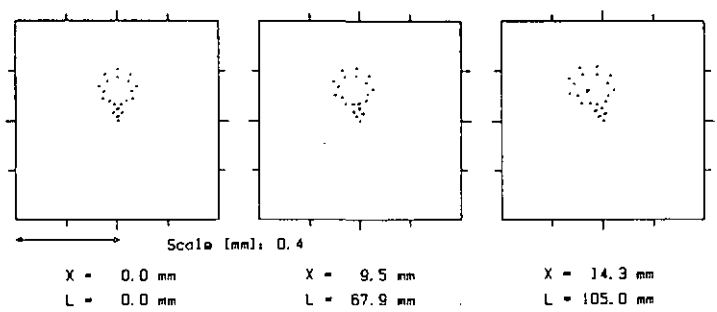

(b)

Fig.3.2. Spot diagrams for three linear hologram positions x, corresponding to the scan lengths L. The geometrical parameters (Fig.3.1) are f = 300 mm, D = 5 mm, ρ = 50 mm, α = 0 deg and

a) γ = 0 deg,

b) γ = -10 deg.

3.2 Disk configuration scanners

Disk configuration scanners are widely used in holographic scanning, because, they are relatively easy to manufacture. In this section, the problem of generating a straight line by a circular motion of a holographic disk scanner will be discussed in detail.

3.2.1 Scan equation and astigmatism

In the case of a circular motion, the hologram rotates around the z-axis (Fig.3.3) with the rotation angle ϕ. The line $\mathbf{x}(s)$ is a circle of radius R and so it is convenient to use ϕ as the scan parameter s in the hologram plane ($\phi = s$). The generated line $\mathbf{y}(t)$ is again a straight line, and the deflection angle β will be used as the scan parameter t in space ($\beta = t$). The generated line is assumed to be parallel to the hologram plane, with the scan plane tangential to the hologram motion, which means that the u-axis is tangential to the circle $\mathbf{x}(s)$ (Fig.3.3). Instead of cartesian coordinates x,y, polar coordinates r,ϕ are introduced in the hologram plane. The derivatives of the phase function Φ in the two coordinate systems r,ϕ and u,v on the circle $\mathbf{x}(s) = (r=R, \phi)$ are then related by

$$\frac{\partial\Phi}{\partial\phi} = R\frac{\partial\Phi}{\partial u}, \qquad \frac{\partial\Phi}{\partial r} = \frac{\partial\Phi}{\partial v}. \tag{3.13}$$

$$\frac{\partial^2\Phi}{\partial\phi^2} = R^2\frac{\partial^2\Phi}{\partial u^2} - R\frac{\partial\Phi}{\partial v}, \quad \frac{\partial^2\Phi}{\partial r\partial\phi} = R\frac{\partial^2\Phi}{\partial u\partial v} + \frac{\partial\Phi}{\partial u}, \quad \frac{\partial^2\Phi}{\partial r^2} = \frac{\partial^2\Phi}{\partial v^2}. \tag{3.14}$$

Introducing these relations into Eqs.(2.9) and (2.10), yields for the derivatives of $\Phi(r,\phi)$ on the scan line (r = R)

$$\frac{\partial\Phi}{\partial\phi} = R\,h_1(\beta), \qquad \frac{\partial\Phi}{\partial r} = h_2(\beta), \tag{3.15}$$

$$\frac{\partial^2\Phi}{\partial\phi^2} = R^2\,h_{11}(\beta) - R\,h_2(\beta), \quad \frac{\partial^2\Phi}{\partial r\partial\phi} = R\,h_{12}(\beta) + h_1(\beta), \quad \frac{\partial^2\Phi}{\partial r^2} = h_{22}(\beta), \tag{3.16}$$

where h_i and h_{ij} are given by the local phase $\Psi(u,v,\beta)$ required for the desired outgoing wave [Eqs.(2.5) and (2.6)].

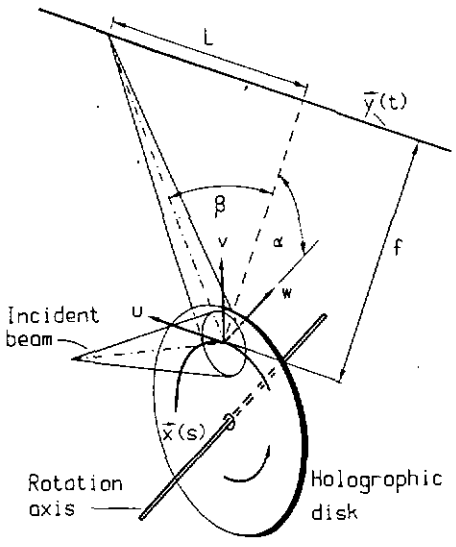

Fig.3.3. Circular motion x(s) of the hologram (rotating disk) to generate a straight line y(t) in space.

As in the case of linear motion, we assume for the phase function $\Phi(r,\phi)$ a second order (parabolic) approximation perpendicular to the scan line. Therefore, the phase function may be written, similar to Eq.(3.5), as

$$\Phi(r,\phi) = k\,[a_0(\phi) + a_1(\phi)\,(r - R) + (1/2)\,a_2(\phi)\,(r - R)^2]. \qquad (3.17)$$

Using second order approximation, the functions $h_i(\beta)$ and $h_{ij}(\beta)$ can be obtained with the help of Eqs.(2.33) and (2.34) for the scan geometry shown in Fig.3.3 with $\delta = 0$. Introducing the results into Eqs.(3.15) and (3.16), yields finally

$$a_0' = R\sin\beta, \quad a_0'' = R^2(a\cos^2\beta - 1/\rho) - R(\sin\alpha\cos\beta - \sin\gamma), \qquad (3.18)$$

$$a_1 = \sin\alpha\cos\beta - \sin\gamma, \quad a_1' = \sin\beta + R(c\cos\alpha\cos\beta - a\sin\alpha\sin\beta\cos\beta), \qquad (3.19)$$

$$a_2 = a\sin^2\alpha\sin^2\beta - 2\,c\sin\alpha\cos\alpha\sin\beta + b\cos^2\alpha - \cos^2\gamma/\rho. \qquad (3.20)$$

with $' = d/d\phi$ and $'' = d^2/d\phi^2$.

Since the relation $a_0'' = d(a_0')/d\phi$ has to be fulfilled, we obtain from Eqs.(3.18) the scan equation

$$d\beta/d\phi - R\, a(\beta) \cos\beta + R/(\rho \cos\beta) + \sin\alpha - \sin\gamma/\cos\beta = 0, \tag{3.21}$$

which determines the relation $\beta(\phi)$ between the scan angle β and the rotation ϕ of the hologram for a given curvature $a(\beta)$ of the outgoing wave in the scan plane. The geometry shown in Fig.3.3 requires for ideal focussing that $a(\beta) = - \cos\beta/f$; therefore, the scan equation becomes

$$d\beta/d\phi = R\,[- \cos^2\beta/f - 1/(\rho \cos\beta)] - \sin\alpha + \sin\gamma/\cos\beta. \tag{3.22}$$

As in the derivation of Eq.(3.21), and since the relation $a_1' = da_1/d\phi$ must be fulfilled, we obtain from Eqs.(3.19)

$$d\beta/d\phi - R\, a(\beta) \cos\beta + 1/\sin\alpha + R\, c(\beta)/(\tan\alpha \tan\beta) = 0. \tag{3.23}$$

Now the scan equation (3.21) and Eq.(3.23) have to be satisfied simultaneously. Thus for c the condition becomes

$$c(\beta) = (\tan\beta/R)[(\tan\alpha/\cos\beta)(R/\rho - \sin\gamma) - \cos\alpha]. \tag{3.24}$$

As can be seen from Eq.(2.23), c essentially determines the astigmatism A of the outgoing wave. It becomes minimal ($|A| = |c|$) for $a = b$; this condition can be satisfied by choosing a_2 from Eq.(3.20) accordingly. As a consequence, there remains an astigmatism $|A| = |c|$, given by Eq.(3.24), with the principal direction $\psi = 45$ deg [Eq.(2.19)]. The astigmatism is equal to zero for $\beta = 0$, but it is not possible to maintain A equal zero for all scan angles β.

Figure 3.4 shows the astigmatism A represented by $c(\beta) \times R$ as a function of the scan angle β for an inclination $\alpha = 45$ deg of the scan plane. In the case of a hologram designed for an incident plane wave ($\rho = \infty$, $\gamma = - 45$ deg, case I), the astigmatism grows continuously with the scan angle β. A better solution can be obtained, if the hologram is designed for a convergent spherical incident wave (case II), which compensates for the astigmatism at the end of the scan. From Eq.(3.24), we find that $\rho/R = - 25$ for $c = 0$ at a scan angle of $\beta = 19$ deg. Alternatively, by changing the angle of the incident wave to $\gamma = 0$ deg, a similar

improved solution can be obtained for a divergent wave of ρ/R = 1.5 (case III). In general, other favorable geometries for minimizing the average astigmatism may be found from Eq.(3.24).

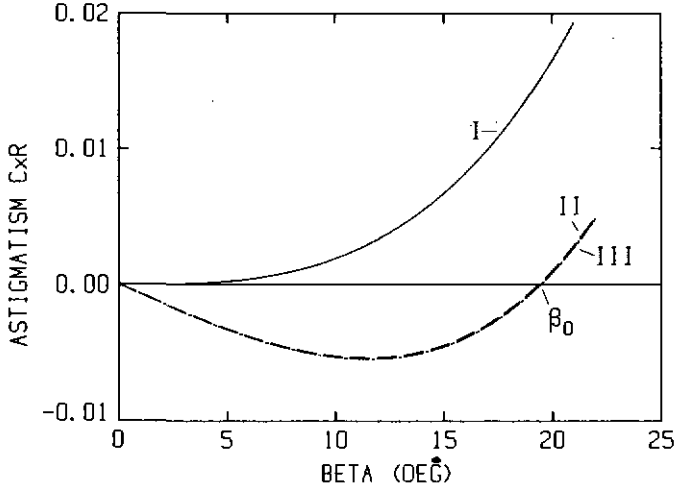

Fig.3.4 Angular dependence of the astigmatism A represented by the product of c(β) × R, where R is the disk radius:

I) Plane incident wave ρ/R = ∞, α = 45 deg, γ = - 45 deg,

II) Convergent incident wave ρ/R = - 25, α = 45 deg, γ = - 45 deg,

III) Divergent incident wave ρ/R = 1.5, α = 45 deg, γ = 0 deg.

As in the case of linear motion, we have applied geometrical ray tracing to the holograms described by Eq.(3.17). The calculations were done for a distance from scan line to hologram of f = 300 mm, a beam diameter D = 5 mm and a radius R = 40 mm in the hologram plane. Figure 3.5(a) shows the results for an incident plane wave (case I) at three different rotation positions ϕ_R of the holographic scanner, namely ϕ_R = 0, 6.2, 12.4 deg, which correspond to β = 0, 9.6, 19.3 deg, respectively. The maximum scan length in the image plane is L = f tanβ = ±105 mm. The arc length on the circle in the hologram plane used for this scan is only ±8.6 mm, which is quite small for a beam diameter D = 5 mm. Therefore, the higher order aberrations are expected to be considerable.

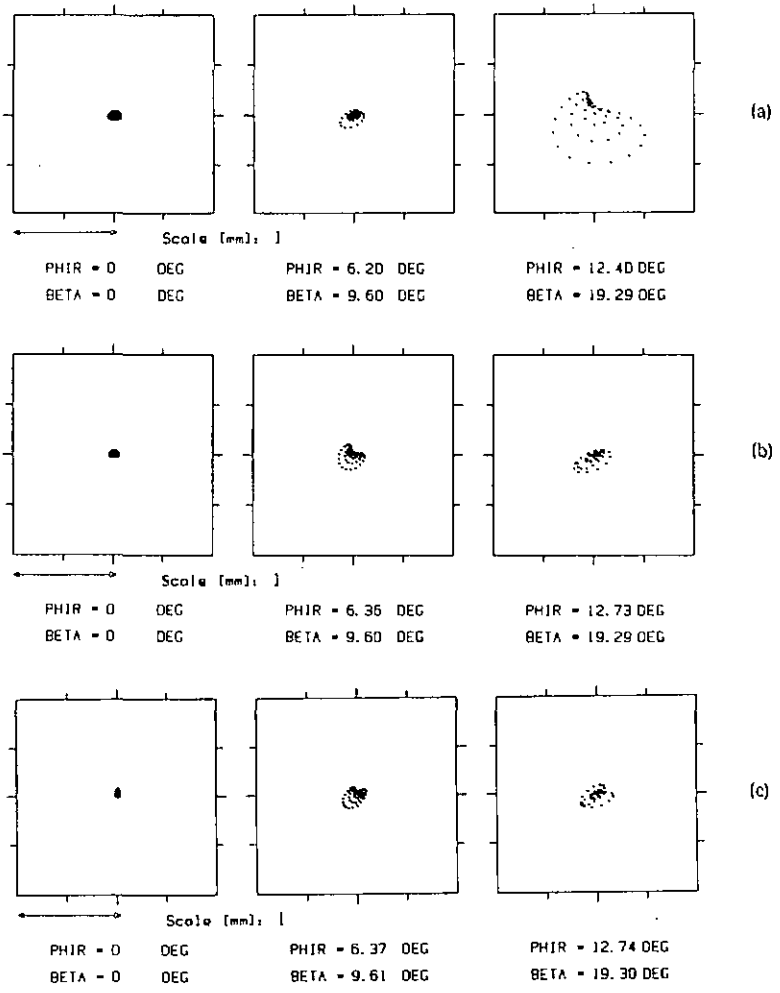

Fig.3. 5. Spot diagrams for three circular hologram positions ϕ_R (PHIR), corresponding to the scan angles β. The geometrieal parameters (Fig.3.3) are f = 300 mm, D = 5 mm, R = 40 mm.

(a) Plane incident wave $\rho = \infty$, $\alpha = 45$ deg, $\gamma = -45$ deg (case I),

(b) Convergent incident wave $\rho = -1000$ mm, $\alpha = 45$ deg, $\gamma = -45$ deg (case II),

(c) Divergent incident wave $\rho = 60$ mm, $\alpha = 45$ deg, $\gamma = 0$ deg (case III).

Figures 3.5(b) and 3.5(c) show the spot diagrams for the better solutions with respect to astigmatism, using a convergent incident wave (ρ = - 1000 mm, case II) and a divergent incident wave (ρ = 60 mm, case III), respectively. The improvement is quite evident.

As seen from Fig.3.5, the focal spots are asymmetric. Although the principle ray follows a straight line, the center of gravity of the spot deviates slightly. Our numerical ray-tracing calculations revealed, that these deviations are less than $\pm 18\ \mu m$ for a beam diameter of D ≈ 5 mm and less than $\pm 8\ \mu m$ for D ≈ 3 mm.

Note that the phase Φ is described up to second order by Eq.(3.17). Equations (3.18) to (3.20) show, that in the direction of the scan line $\mathbf{x}(s) = (r=R, \phi)$, the solutions for Φ are completely determined by the first and the second order terms, whereas, perpendicular to the scan line, corrections with higher order terms are still possible. We shall explore the effect of such higher order terms in chapter 5.

3.2.2 Discussion of astigmatism

The function $c(\beta)$ [Eq.(3.24)] essentially determines the astigmatism A of the outgoing wave by Eq.(2.23). We shall now consider $c(\beta)$ and its influence on the spot quality during scanning in greater detail. The astigmatism can be minimized for many of different geometrical arrangements. Instead of checking them all, we shall first extract the basic parameters of $c(\beta)$, and then determine their behaviour for representative arrangements.

Equation (3.24) shows that $c(\beta)$ is an odd function, so that $c(\beta) = - c(-\beta)$. In general, as shown in Fig.3.4, the functions $c(\beta)$ are equal to zero at the origin (β = 0) and again at another angle β_0; for the special case of curve i in Fig.3.4, β_0 is also equal to 0. Introducing β_0 as a parameter, Eq.(3.24) can be simplified to

$$c(\beta) = (\tan\beta \cos\alpha/R)[(\cos\beta_0/\cos\beta) - 1], \qquad (3.25)$$

where

$$\cos \beta_0 = (\tan\alpha/\cos\alpha)\,[(R/\rho) - \sin\gamma]. \qquad (3.26)$$

During the scan motion the disk rotates around its axis and β increases up to a maximum given by the total scan length. Thus, in Eq.(3.25) three remaining basic parameters can be modified in order to reduce the astigmatism: (1) the angle β_0, where $c(\beta)$ is zero, (2) the inclination α of the outgoing wave and (3) the disk radius R. Note that all disk configurations, regardless of their geometry, which have the same basic parameters, will have the same astigmatism. For example, in the two cases shown in Fig.3.4, one has a convergent incident wave at $\gamma = 45$ deg (case II) and the other a divergent incident wave at $\gamma = 0$ deg (case III), yet their astigmatism [$c(\beta)$] behaviors are identical.

Equation (3.25) shows, that the astigmatism decreases with an increasing α and disappears for $\alpha \rightarrow 90$ deg. Also, that the astigmatism varies linearly with the disk radius R. However, in addition to astigmatism, there are other factors that influence the spot quality; for example, higher order aberrations and the pupil size. Therefore, to include the effects of the pupil size and higher order aberrations, the holographic disk scanners are analyzed with the aid of the ray tracing method explained in the Appendix.

Using the ray tracing method, the spot quality can be represented by the spot diagrams, as shown, for example, in Fig.3.5. The points in this diagrams, given by the vectors $\mathbf{x}_i = (x_i, y_i)$, are the intersection points of the traced rays with the image plane. To compare the quality of the different spot diagrams, a merit function for aberration E_A, is introduced

$$E_A = [(\sum_{i=1}^{N} |\mathbf{x}_i - \langle \mathbf{x}_i \rangle|^2/N)_j]_{max}, \qquad j = 1,2, \ldots, M, \qquad (3.27)$$

where $\langle \mathbf{x}_i \rangle = \sum \mathbf{x}_i/N$ is the gravity point of the spot diagram, N the number of rays (index i) traced for each scan position and M is the number of positions (index j). In general, the function E_A is determined for several positions of rotation, uniformly distributed over the hologram; from the origin $\phi_R = 0$, ($\beta = 0$) to the maximum scan angle. In our case, the function E_A was calculated for 5 scan positions, and at each position a bundle of 49 rays was traced.

We shall now discuss the influence of the basic parameters β_0, α and R on the astigmatism [Eq.(3.25)] as well as to the spot quality (ray tracing) for some typical examples. Especially disk scanners are considered with radius R = 40 mm, hologram to scan line distance f = 300 mm and an exit pupil diameter D = 5 mm (for $\beta = 0$). The exit pupil is kept constant for the different scanner geometries, so as to always compare solutions with the same diffraction limited spot size. The scan length L is related to the deflection angle β by $L = f \tan\beta$ (Fig.3.3), where L = ±105 mm and $\beta = \pm 19.3$ deg at the end of the scan. The wavelength λ appears as a scale factor ($k = 2\pi/\lambda$) in the hologram phase function $\Phi(r,\phi)$ given by Eq.(3.17); therefore, λ does not influence the corrections.

1) Influence of β_0

Earlier we arbitrarily set β_0 at 19 deg. Now we shall vary β_0 continuously to determine, in more detail, its influence on the spot quality. Two different geometrical disk configurations were considered. One was a symmetrical arrangement with an incident plane wave $\rho = \infty$ and $\alpha = -\gamma$. The variation of β_0 was achieved by varying α ($= -\gamma$) according to Eq.(3.26). This arrangement is advantageous for realizing high efficiency volume holograms; the fringes in the holographic emulsion are approximately perpendicular to the hologram plane (exactly perpendicular in the center) and so, emulsion shrinkage does not change the grating geometry. The other configuration was non-symmetrical with $\alpha = 45$ deg and $\gamma = 0$ deg, so the incident wave was parallel to the rotation axis of the disk. Here, the variation of β_0 was achieved by changing the curvature ρ of the incident wave [Eq.(3.26)]. The calculated results of the merit function for the two configurations were very similar, so only the results for the symmetrical arrangement are given in Fig.3.6. As shown, the minimum occurs at $\beta_0 = 19.5$ deg, which is near the scan end β_E (= 19.3 deg).

The behaviour of the astigmatism A, described by $c(\beta)$, for the minimum ($\beta_0 = 19.5$ deg) is presented in Fig.3.7. Starting at the origin, the function $c(\beta)$ grows to an extremum, changes its direction, strikes the zero-axis at β_0 and grows again until the edge of the aperture in the hologram plane at ϕ_p, which corresponds to the deflection angle β_p.

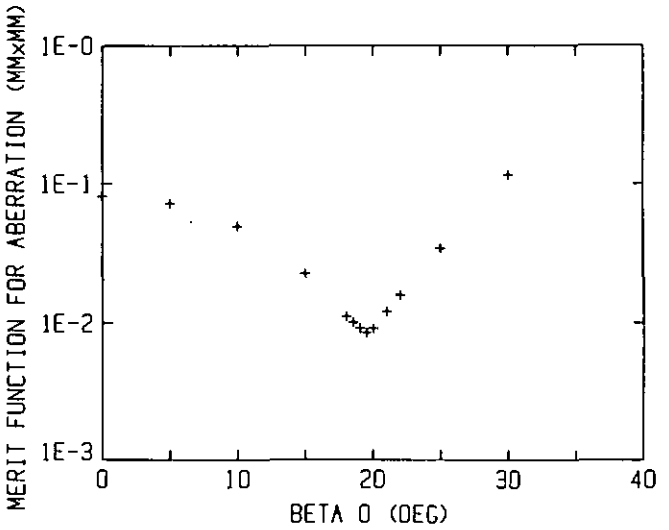

Fig.3.6. Merit function for aberration versus β_0 (BETA 0), for an incident plane wave $p = \infty$ and a symmetrical configuration $\alpha = -\gamma$.

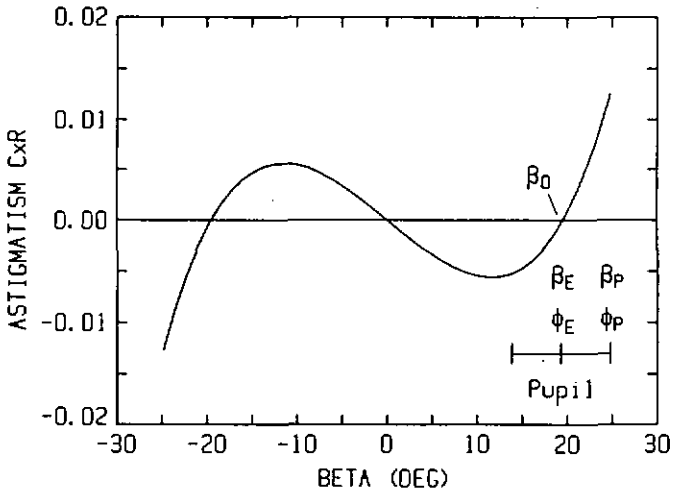

Fig.3.7. Astigmatism, represented by $c(\beta) \times R$, as a function of β. The incident wave is a plane wave with $p = \infty$ and the angles are $\alpha = -\gamma = 44.15$ deg ($\beta_0 = 19.5$ deg).

Figure 3.8 shows the spot diagrams for the best solution with respect to the merit function E_A for the symmetrical configuration, using an incident plane wave $\rho = \infty$ and the angles $\alpha = -\gamma = 44.15$ deg ($\beta_0 = 19.5$ deg). There are few aberrations in the scan center $\phi_R = 0$, and then the aberrations increase. Nevertheless, the spots remain still well concentrated. The standard deviations $\langle r_i^2 \rangle^{1/2}$ of the spot distributions are less than 92 μm. As a consequence of balancing the aberrations, the spot quality at $\phi_R = 6.28$ deg is equivalent to the spot quality at the end of the scan, $\phi_R = 12.57$ deg.

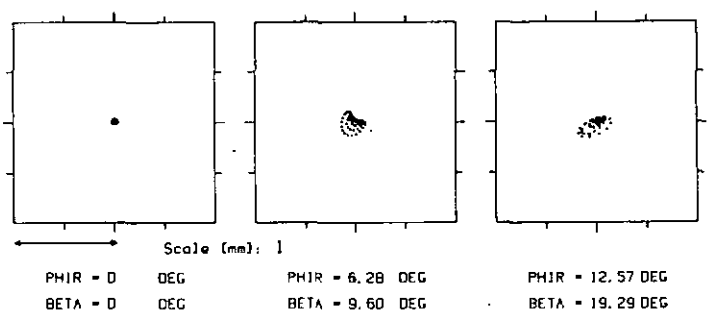

Fig.3.8. Spot diagrams for three circular hologram positions ϕ_R (PHIR), corresponding to the scan angles β. The geometrical parameters (Fig.3.3) are f = 300 mm, D = 5 mm, $\rho = \infty$, $\alpha = -\gamma = 44.15$ deg. The maximum scan length $L = f \tan\beta$ is ±105 mm.

2) Influence of α

The angle α is the inclination of the scan plane (Fig.3.3), the plane in which the principal ray moves during scanning. We calculated the merit function for aberration E_A as a function of α, with $\beta_0 = \beta_E = 19.3$ deg. These calculations were again performed for two geometrical configurations, and the results are shown in Fig.3.9. Curve I (marked with 'o') describes the symmetrical arrangement with $\alpha = -\gamma$ and curve II (marked with '+') describes the non-symmetrical

configuration with $\gamma = 0$ deg. In both cases the curvature ρ of the ineident beam was varied simultaneously with α to keep the position of β_0 at 19.3 deg [Eq.(3.26)]. Following Eq.(3.25) for the astigmatism, the aberrations should improve for an inereasing angle α. This is true until a minimum value is reaehed, but then the spot quality becomes worse again.

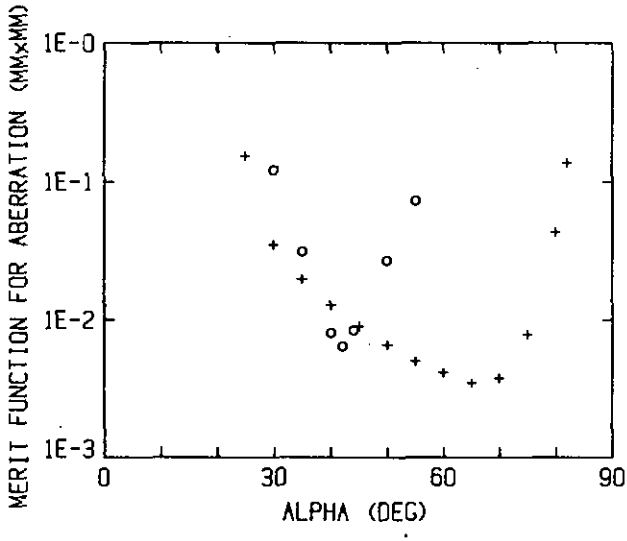

Fig.3.9. Merit function for aberration versus α.

I) Symmetrical case with $\alpha = -\gamma$, (o).

II) Nonsymetrical case with $\gamma = 0$, (+).

The inereasing values for the merit function for larger α values can be explained by the following reasoning:

When α inereases to 90 deg, the astigmatism decreases to zero according to the funetion eosα, as given in Eq.(3.25); thus the slope of e(α) at 90 deg is linear. On the other hand, the influence of the astigmatism (and higher order terms) on the spot quality depends strongly on the aperture. In our case, the pupil diameter D of the outgoing wave was kept constant to ensure a constant diffraetion from the aperture. Thus, the illuminated spot on the disk grows

towards infinity with D/cosα in the y-direction, with a slope, which is also infinite. As a result, the increase of the aberrations, due to the aperture effects, is much stronger than the decrease of the cosine function, so the merit function becomes worse.

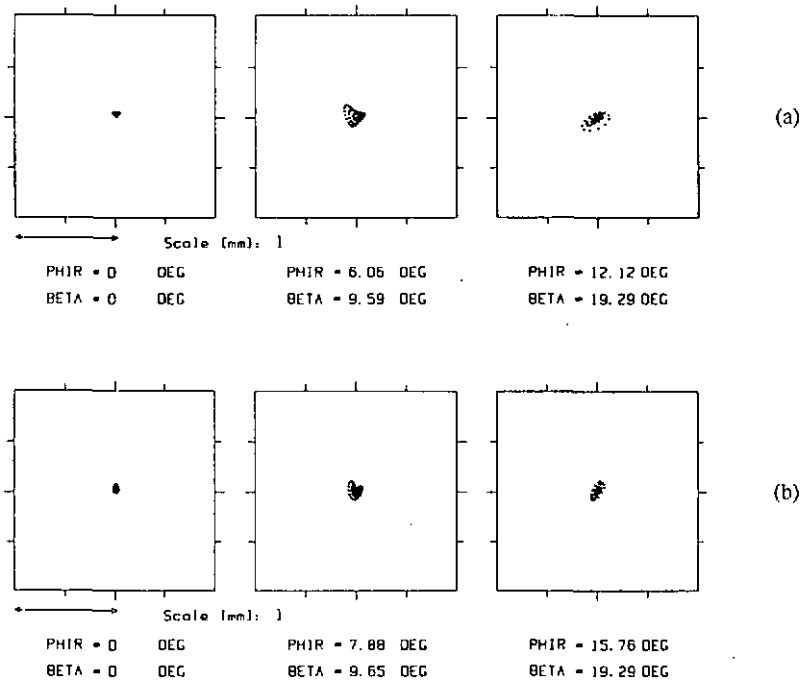

Fig.3.10. Spot diagrams for three circular hologram positions ϕ_R (PHIR), corresponding to the scan angles β. The geometrical parameters (Fig.3.3) are f = 300 mm, D = 5 mm and for the two cases:
a) ρ = 364 mm, α = -, γ = 42.0 deg, symmetrical configuration.
b) ρ = 215 mm, α = 65 deg, γ = 0 deg, non-symmetrical configuration.
The maximum scan length L = f tanβ is ±105 mm.

The spot diagrams at the minima positions of α for the two configurations were also calculated, and the results are presented in Fig.3.10. Figure 3.10a shows the spot diagrams for the symmetrical configuration with $\alpha = -\gamma = 42.0$ deg and a divergent incident wave $\rho = 364$ mm. Figure 3.10b shows a non-symmetrical configuration with $\alpha = 65$ deg, $\gamma = 0$ deg and a divergent wave $\rho = 215$ mm. The standard deviations $\langle r_i^2 \rangle^{1/2}$ of the spot distributions were found to be less than 80 μm for the symmetrical configuration and less than 59 μm for the better non-symmetrical configuration.

3) Influence of the disk radius R

Equation (3.25) indicates, that the astigmatism varies linearly with the disk radius R. This is not so for the spot quality, as can be seen in Fig.3.11. Here the influence of the disk radius R on the spot quality, described by the merit function for aberration, is shown. Curve I depicts the results for a pupil diameter of D = 5 mm (marked with 'o'), whereas curve II is for D = 10 mm (marked with '+'). The calculations were made for an incident plane wave $\rho = \infty$, and the angles $\alpha = -\gamma = 44.17$ deg ($\beta_0 = 19.3$ deg). By increasing R, the spot quality becomes better, but then, we can observe a saturation for large radii. Note, that even for a diameter of D = 10 mm, it is already necessary to work with a very large disk.

The length of the scan path in the hologram plane, necessary to generate a given scan length L, grows with the disk radius R, if $d\beta/d\phi$ is independent of R. A longer scan path simplifies the corrections, because the overlapping area in the hologram plane between two scan positions is smaller. From Eq.(3.22) it follows, that in the case of an incident plane wave $\rho = \infty$, $d\beta/d\phi$ varies slowly with R, when $R << f$. For larger R, $d\beta/d\phi$ increases, thereby limiting the scan path. For large disk radii a linear translation scanner (section 3.1) is approached, and R no longer influences the spot quality.

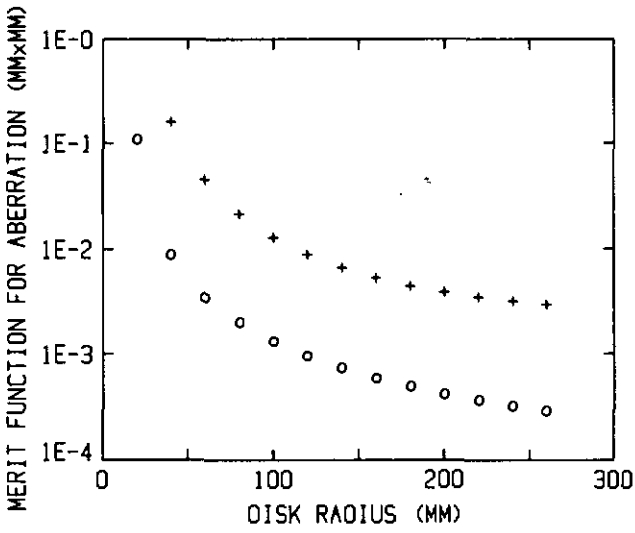

Fig.3.11. Merit function for aberration versus the disk radius R, for an incident plane wave $\rho = \infty$ and the angles $\alpha = -\gamma = 44.17$ deg. The pupil diameters are D = 5 mm, (o) and D = 10 mm, (+).

Concluding remarks

By taking the problems associated with the aperture size and higher order aberrations into account, advantageous geometrical arrangements for holographic disk scanners can be deduced from Eq.(3.25), which describes the astigmatism. We found that configurations with the same basic parameters β_0, α, and R have identical behaviour with respect to astigmatism, but their behaviour may differ with respect to the spot quality. Consequently, in addition to the astigmatism, it is necessary to include the spot quality, using the ray tracing method, when designing holographic disk scanners.

3.2.3 Curved scan line

In sections 3.2.1 and 3.2.2 we considered the generation of a straight line for disk configuration scanners. There, the principal ray always describes a straight line and remains in the scan plane with an inclination of α = constant. In practice, the generated line must remain straight within some tolerance limits. For point of sale systems the tolerances are fairly large, so that even uncorrected systems are suitable [1]. However, for laser printer applications, the required tolerances are more stringent. For example, they must not exceed 100 µm for a total scan length of at least 200 mm. In this section we shall consider the relation between deviation from a straight line and astigmatism; and show that, by alleviating the requirements for straightness, it is possible to improve the spot quality. Astigmatism free, axial symmetric configurations to generate curved lines, were reported in the literature [7,8]. These lines are always circles centered at the rotation axis, and are therefore strongly curved. The question is, whether there are other solutions with less deviations.

For a curved line, the principal ray does not move in a plane, so $\alpha(\phi)$ becomes a function of ϕ. Nevertheless, the basic Eqs.(3.18) to (3.20) for a disk scanner are still valid. By exploiting the derivatives of the coefficients a_0 and a_1, it is possible to develop the scan equation [Eq.(3.22)] and the equation for astigmatism [Eq.(3.24)], with $\alpha = \alpha(\phi)$. The scan equation remains the same as Eq.(3.22), but the equation for the astigmatism changes to

$$R\, c(\beta(\phi)) = \tan\beta\, [(\tan\alpha/\cos\beta)(R/\rho - \sin\gamma) - \cos\alpha] + d\alpha/d\phi. \qquad (3.28)$$

where $d\alpha/d\phi$ is an additional term, which allows us to compensate for the astigmatism. In particular, $c(\beta) = 0$ requires

$$d\alpha/d\phi = -\tan\beta\, [(\tan\alpha/\cos\beta)(R/\rho - \sin\gamma) - \cos\alpha]. \qquad (3.29)$$

This differential equation can be solved for $\alpha(\phi)$ to yield

$$\alpha(\phi) = \alpha_c + \Delta\alpha(\phi), \qquad (3.30)$$

where α_c is a constant deflection angle. The deviation of the generated line in the image plane is now given by $\Delta y = f \tan(\Delta\alpha)$.

The derivative $d\alpha/d\phi$ compensates for the typical astigmatism $c[\beta(\phi)]$, depicted in Fig.(3.7). A larger astigmatism leads to a stronger curved scan line. In chapter 3.2.2 the scan angle β_0, where the astigmatism disappears, was introduced as a useful optimizing parameter. In the case of a curved scan line, it is necessary to redefine β_0, or the corresponding value ϕ_0, as the value where $d\alpha/d\phi$ disappears. For small variations of $\alpha(\phi)$, β_0, obtained by this new definition, is nearly identical to the value determined by equation (3.26), where the astigmatism disappears.

The position of β_0 (or ϕ_0) now influences the line straightness. For straight line scanning, β_0 is set near to the end β_E of the scan in order to minimize the aberrations. For a curved scan line, for which the astigmatism can be eliminated, a new position of β_0 has to be found in order to minimize the deviation.

Similar to the merit function for aberration E_A [Eq.(3.27)], a merit function for lincarity E_L is introduced to assess the deviation from a straight line, namely

$$E_L = [(Y_j - \langle Y_j \rangle)^2]_{max}, \qquad j = 1.2. \ldots ,M, \tag{3.31}$$

were $Y_j = \langle y_i \rangle_j = \Sigma\, y_i/N$ is the mean value for one scan position, N is the number of rays (index i) traced for each scan position and M is the number of positions (index j). The vectors $\mathbf{x}_i = (x_i, y_i)$ are the points of intersection of the traced rays with the image plane. Since the generated scan line is parallel to the x-axis, only y_i is of interest for linearity. The merit function E_L becomes minimal for a minimal deviation from the straight line generated by the holographic disk. For our calculations 5 scan positions, each with 49 rays, were considered.

We calculated the merit function for linearity E_L as a function of the angle β_0 for the same disk geometry as before. Specifically, the diameter of the exit pupil was D = 5 mm, the hologram to scan line distance was f = 300 mm and the disk radius was R = 40 mm. A symmetrical case $\alpha = -\gamma$ was established, using an incident plane wave ($\rho = \infty$). Figure 3.12 shows the results. The minimum of the merit function is found at $\beta_0 = 13.5$ deg $= 0.7\,\beta_E$. The values of $\Delta\alpha$ and $d\alpha/d\phi$ as functions of ϕ were also determined and the results are sketched in Fig.3.13. The variation of Δy in the image plane, is balanced until the end of the scan,

whereby $\Delta y = f \tan[\Delta\alpha(\phi)]$. In fact $\Delta\alpha(\phi)$, which gives the angle for the principal ray, is not exactly zero at the end of the scan. This is due to the definition of the merit function, which sets the center of gravity of the spot diagram as the center of the spot and not the principal ray.

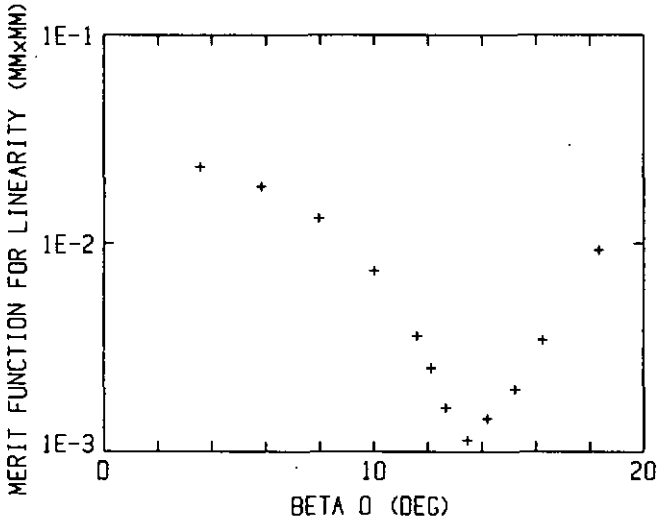

Fig.3.12. Merit function for linearity versus β_0, for $\alpha = -\gamma$ and an incident plane wave $\rho = \infty$.

When the astigmatism is compensated for, the spot quality should be improved. This is indeed confirmed by the spot diagrams shown in Fig.3.14. The calculations were performed for an incident plane wave $\rho = \infty$, and with $\alpha_C = -\gamma = 44.6$ deg. Note that the standard deviations $\langle r_i^2 \rangle^{1/2}$ of the spot distributions are less than 53 μm, which is better than for the corresponding case of straight line scanning (Fig.3.8), where the standard deviations were as large as 92 μm. The total calculated variation of the scan line is less than ±30 μm.

By allowing small deviations from a straight line, it is possible to compensate for the astigmatism of a disk configuration scanner. If the astigmatism is large, then the deviation becomes large. This additional flexibility opens many possibilities in scanner design and optimization.

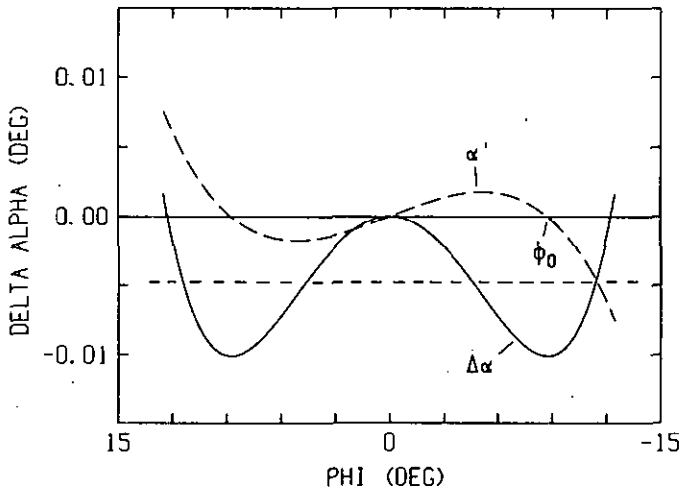

Fig.3.13. Variation of $\Delta\alpha(\phi)$ and $d\alpha/d\phi$ as a function of ϕ, when the astigmatism is compensated. The incident wave is a plane wave with $\rho = \infty$ and the angles are $\alpha = -\gamma = 44.6$ deg.

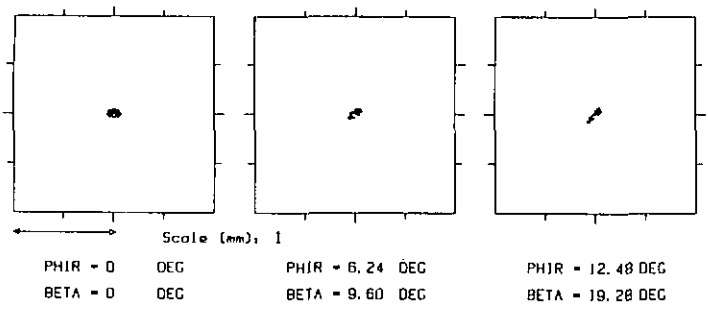

Fig.3.14. Spot diagrams for three circular hologram positions ϕ_R (PHIR) corresponding to the scan angles β. The geometrical parameters are f = 300mm, D = 5 mm, $\rho = \infty$, $\alpha = -\gamma = -44.6$ deg. The maximum scan length $L = f \tan\beta$ is ± 105 mm.

3.3 Drum configuration scanner

Our analytical design method for holographic scanning elements is not limited to planar holographic substrates. For example, the method can be applied to a drum configuration scanner, where the holographic substrate is a cylinder (Fig.3.15). Such a configuration simplifies the problem of straight line scanning, because the output beam remains in a plane orthogonal to the rotation axis [8]. In this section, we shall develop the scan equation and the equation for the astigmatism of a drum configuration scanner.

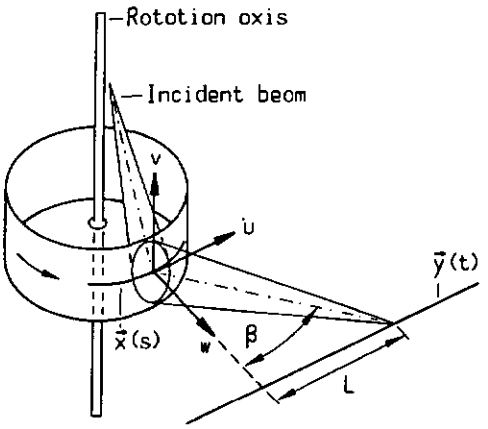

Fig.3.15. Drum configuration scanner.

Figure 3.15 shows the basic geometry of a drum configuration scanner. The cylinder turns around its axis, with the rotation angle of ϕ. The line $\mathbf{x}(s)$ is a circle of radius R equal to the radius of the drum. Therefore, it is convenient to use ϕ as the scan parameter s in the hologram surface ($\phi = s$). The generated line $\mathbf{y}(t)$ is again a straight line and the deflection angle β will be used as the scan parameter t in space ($\beta = t$). The generated line is assumed to be perpendicular to the cylinder axis and the u-axis of the local coordinate system is tangential to the circle $\mathbf{x}(s)$. Instead of the cartesian coordinates x,y,z, the cylindrical coordinates ϕ, r, y are introduced. On the hologram surface r = R and

therefore, ϕ,y are the appropriate variables. The derivatives of Φ in the two coordinate systems ϕ,r,y and u,v,w on the circle $\mathbf{x}(s) = (\phi, r = R, y = 0)$ are then related by

$$\frac{\partial\Phi}{\partial\phi} = R\frac{\partial\Phi}{\partial u}, \qquad \frac{\partial\Phi}{\partial y} = \frac{\partial\Phi}{\partial v}, \tag{3.32}$$

$$\frac{\partial^2\Phi}{\partial\phi^2} = R^2\frac{\partial^2\Phi}{\partial u^2} - R\frac{\partial\Phi}{\partial w}, \qquad \frac{\partial^2\Phi}{\partial y\partial\phi} = R\frac{\partial^2\Phi}{\partial u\partial v}, \qquad \frac{\partial^2\Phi}{\partial y^2} = \frac{\partial^2\Phi}{\partial v^2}. \tag{3.33}$$

Since the hologram surface is not identical with the u,v-plane of the local coordinate system, the derivative with respect to w also appears in Eq.(3.33). Introducing Eqs.(3.32) and (3.33) into Eqs.(2.9) and (2.10), yields for the derivatives of $\Phi(\phi,y)$ on the scan line (r = R)

$$\frac{\partial\Phi}{\partial\phi} = R\,h_1, \qquad \frac{\partial\Phi}{\partial y} = h_2, \tag{3.34}$$

$$\frac{\partial^2\Phi}{\partial\phi^2} = R^2\,h_{11} - R\,h_3, \qquad \frac{\partial^2\Phi}{\partial y\partial\phi} = R\,h_{12}, \qquad \frac{\partial^2\Phi}{\partial y^2} = h_{22}. \tag{3.35}$$

where h_i and h_{ij} (i,j = 1,2) are given by the local phase $\Psi(u,v,\beta)$ required for the desired outgoing wave [Eqs.(2.5) and (2.6)] and similarly $h_3 = (\partial\Psi/\partial w)$.

As for the linear translation and disk scanners, we assume for the phase function $\Phi(\phi,y)$ a second order (parabolic) approximation perpendicular to the scan line. Therefore, the phase function may be written similar to Eq.(3.5) as

$$\Phi(\phi,y) = k\,[a_0(\phi) + a_1(\phi)\,y + (1/2)\,a_2(\phi)\,y^2]. \tag{3.36}$$

Using second order approximation, the functions $h_i(\beta)$ and $h_{ij}(\beta)$ can be obtained with the help of Eqs.(2.33) and (2.34) for the scan geometry shown in Fig.3.15 when $\alpha \neq 0$ and $\delta = 0$. Although h_3 has not been calculated explicitly in chapter 2.3, it can be obtained similarly from Eq.(2.25). This can be done by replacing α and β with γ and $\delta = 0$ for the incident beam, to yield

$$h_3 = k(\cos\alpha\cos\beta - \cos\gamma). \tag{3.37}$$

Introducing the results into Eqs.(3.34) and (3.35), yields

$$a_0' = R\sin\beta. \quad a_0'' = R^2(a\cos^2\beta - 1/\rho) - R(\cos\alpha\cos\beta - \cos\gamma). \tag{3.38}$$

$$a_1 = \sin\alpha\cos\beta - \sin\gamma, \quad a_1' = R(c\cos\alpha\cos\beta - a\sin\alpha\sin\beta\cos\beta). \tag{3.39}$$

$$a_2 = a\sin^2\alpha\sin^2\beta - 2c\sin\alpha\cos\alpha\sin\beta + b\cos^2\alpha - \cos^2\gamma/\rho. \tag{3.40}$$

with $' = d/d\phi$ and $'' = d^2/d\phi^2$.

Since the relation $a_0'' = d(a_0')/d\phi$ has to be fulfilled, we can then obtain from Eqs.(3.38) the scan equation

$$d\beta/d\phi - R\,a(\beta)\cos\beta + R/(\rho\cos\beta) + \cos\alpha - \cos\gamma/\cos\beta = 0. \tag{3.41}$$

Equation (3.41) determines the relation between the scan angle β and the rotation ϕ of the holographic cylinder for a given curvature $a(\beta)$ of the outgoing wave in the scan plane. The geometry shown in Fig.3.15 requires for ideal focussing $a(\beta) = -\cos\beta/f$, and, therefore, the scan equation becomes

$$d\beta/d\phi = R\,[-\cos^2\beta/f - 1/(\rho\cos\beta)] - \cos\alpha + \cos\gamma/\cos\beta. \tag{3.42}$$

As in the derivation of Eq.(3.41), it is also necessary to fulfill $a_1' = da_1/d\phi$. Then, from Eqs.(3.39) we obtain

$$d\beta/d\phi - R\,a(\beta)\cos\beta + R\,c(\beta)/(\tan\alpha\tan\beta) = 0. \tag{3.43}$$

Since the scan equation (3.41) and Eq.(3.43) have to be satisfied simultaneously, then for c the condition becomes

$$c(\beta) = [\tan\alpha\tan\beta/(R\cos\beta)]\,[(R/\rho) + \cos\alpha\cos\beta - \cos\gamma]. \tag{3.44}$$

As can be seen from Eq.(2.23), $c(\beta)$ determines essentially the astigmatism A of the outgoing wave. It becomes minimal ($|A| = |c|$) for $a = b$. This condition can be satisfied by choosing $a_2(\phi)$ from Eq.(3.40) accordingly. Yet, there remains an astigmatism $|A| = |c|$, given by Eq.(3.44). If the scan plane is perpendicular to

the cylinder axis ($\alpha = 0$), as sketched in Fig.3.15, then even this astigmatism can be reduced to zero for all scan angles β. This result is not surprising and could also have been derived from simple geometrical considerations. It shows that the outgoing beam has to be normal to the hologram surface and perpendicular to the rotation axis, as it was proposed in the literature [8].

4. EXPERIMENTAL INVESTIGATIONS

This chapter reports the experimental investigations of our calculated holographic disk scanners, which were recorded with the aid of computer generated holograms (CGHs). First the set-ups for recording and reconstruction will be described. Then the experimental results for three different disk scanners will be presented.

4.1 Realization of the holographic scanners

For given readout geometry and wavelength λ_r, the holographic scanner phase function $\Phi(x,y)$ can be calculated according to Eq.(3.17). The phase Φ is formed by recording the interference of a spherical object wave Φ_O and an aspherical reference wave Φ_R at the recording wavelength λ_R ($\neq \lambda_r$). The relation between the phases in the hologram plane is then given by

$$\Phi = \Phi_O - \Phi_R \,. \tag{4.1}$$

The spherical wave Φ_O is chosen, so that the Bragg-condition is fulfilled and that the spatial bandwith of the aspherical wave Φ_R is low. The aspherical wave is generated with the aid of a CGH.

The experimental set-up for recording is shown in Fig.4.1. The laser beam is split into a plane wave branch for the reference wave and a spherical branch for the object wave. The CGH is inserted into the plane wave branch of the recording set-up. A telescopic lens system creates an image 1:1 of the CGH at the holographic scanner, which is inclined with respect to the CGH image plane. The phase function Φ_{CGH} necessary to generate Φ_R in the hologram plane, can be calculated with the aid of the ray tracing method, taking into account the optical path length between the CGH image plane and the hologram plane (Appendix). The carrier frequency ν of the CGH, which is a binary hologram, separates the higher-order wave fronts from the zero order, so that by using a spatial filter, only the first order is allowed to pass, thereby forming the desired aspherical wave.

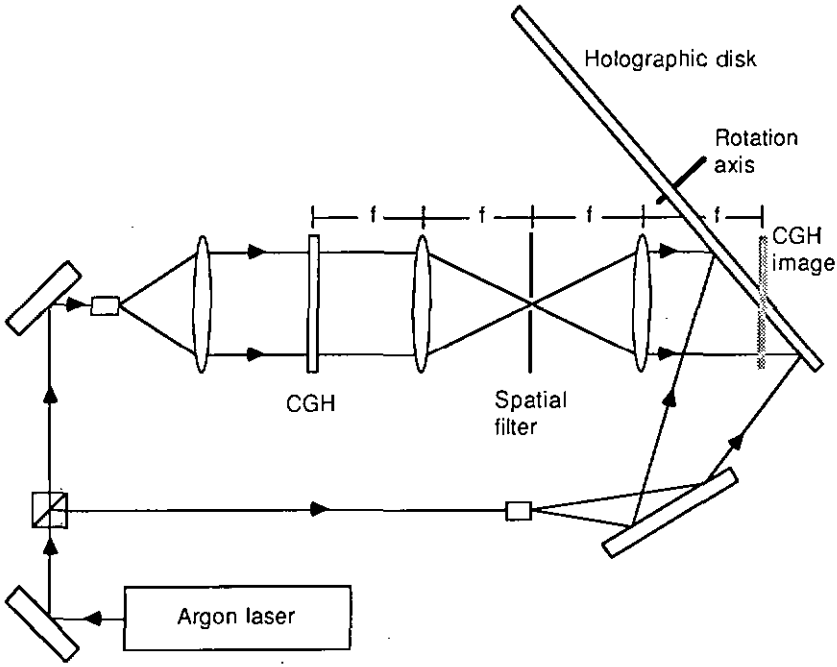

Fig.4.1 Recording set-up to realize a holographic scanning element with the aid of a computer generated hologram (CGH).

The CGH also includes a correction for the change in wavelength between recording and readout of the scanning element [23]. The wavelength shift is imposed because the spectral sensitivity of the high efficieney photosensitive materials is typically < 520 nm, whereas the wavelength of the readout sources, used for the laser scanners, are > 630 nm (e.g. He-Ne, AlGaAs).

In order to obtain high diffraction efficieney for the holographic scanners, the Bragg-condition has to be fulfilled [24]. The Bragg-condition requires for the wavevectors

$$\mathbf{k}_P - \mathbf{k}_r = \mathbf{k}_O - \mathbf{k}_R, \tag{4.2}$$

where $|\mathbf{k}_r| = |\mathbf{k}_p| = 2\pi/\lambda_r$ and $|\mathbf{k}_R| = |\mathbf{k}_O| = 2\pi/\lambda_R$. Note, that P stands for the

reconstructed outgoing wave, r for the reconstructing incident wave, O for the object wave and R for the recording reference wave. We chose our geometry, so that Eq.(4.2) is satisfied for the principle rays in the scan position of zero deflection. Thus, the Bragg-condition yields the direction $\mathbf{k}_O$ of the spherical object wave Φ_O in Eq.(4.1).

The radius ρ_O was chosen to minimize the spatial bandwith of the aspherical wave Φ_R, generated by a CGH. The CGH is a thin binary hologram, that is recorded with the aid of a computer. The phase detour method of Brown and Lohmann [25] was applied to represent the CGH phase function. The calculated structure was drawn with a Benson plotter and photographically reduced (24 ×) to the final size (26 mm × 26 mm). An enlarged section of a CGH is shown in Fig.4.2. The total number of lines of the CGH, the space-bandwith product, that can be generated, depends on the capability of the computer output device. In our experiments the space-bandwith product was 768 lines. This limits the spatial carrier frequency ν of the CGH to ν = 30 lines/mm. On the other hand, the carrier frequency ν has to be high enough to avoid overlapping between the first and the second diffraction order in the frequency plane, where the first order wanted has to be filtered (Fig.4.1). This condition is fulfilled [14], if

$$\nu > 1.5\ U, \tag{4.3}$$

where U is the spatial bandwith of the desired aspherical wavefront. As a consequence, U has to be kept as low as possible. To minimize the spatial bandwith of the aspherical wave, the curvature $1/\rho_O$ of the spherical object wave Φ_O in Eq.(4.1) must be chosen so that the aspherical wave Φ_R will be as close to a plane wave as possible.

A wavelength shift between recording and reconstruction causes mainly a strong astigmatism [23], which must be compensated for by the CGH. The astigmatism can be described with the aid of the second order theory [22]. In the case of hologram recording and reconstruction, where the wavevectors $\mathbf{k}_i$ are in a common plane, the curvatures $1/\rho_i$ are related by

$$\begin{aligned} k_r(\cos^2\theta_p/\rho_p^{\parallel} - \cos^2\theta_r/\rho_r^{\parallel}) &= k_R(\cos^2\theta_O/\rho_O^{\parallel} - \cos^2\theta_R/\rho_R^{\parallel}), \\ k_r(1/\rho_p^{\perp} - 1/\rho_r^{\perp}) &= k_R(1/\rho_O^{\perp} - 1/\rho_R^{\perp}). \end{aligned} \tag{4.4}$$

The curvatures $1/\rho_i^{\perp}$ are perpendicular to the plane of incidence, whereas $1/\rho_i^{\parallel}$ are parallel to the plane. The angles θ_i are between the wavevectors $\mathbf{k}_i$ and the hologram normal. The radius of the spherical wave $\rho_O = \rho_O^{\parallel} = \rho_O^{\perp}$ was chosen, that the mean curvature $1/\rho_m = (1/\rho_R^{\parallel} - 1/\rho_R^{\perp})$ of the astigmatic wave is eliminated; this choice reduces the spatial bandwith of the aspherical wave.

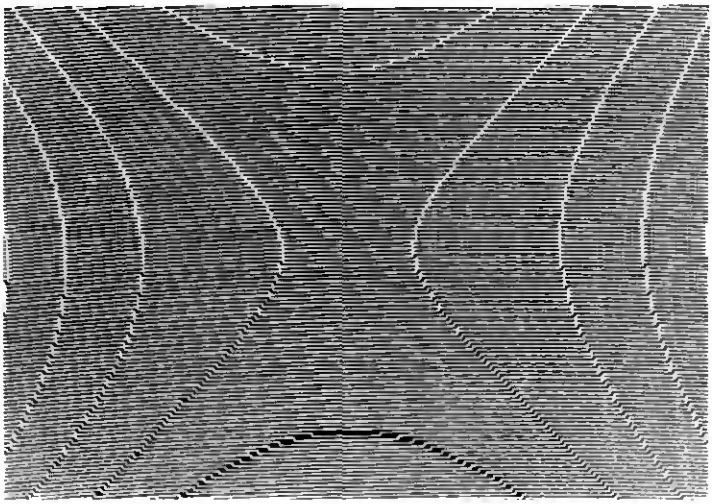

Fig.4.2 Section of the CGH*, drawn with a Benson plotter.

* Recorded by H. Buczek and J. M. Teijido at the CSEM, Neuchâtel, Switzerland.

4.2 Experimental set-up for measuring the performance of the scanners

In the following we shall describe the experimental set-up for measuring the image spot quality and its position with respect to a straight scan line.

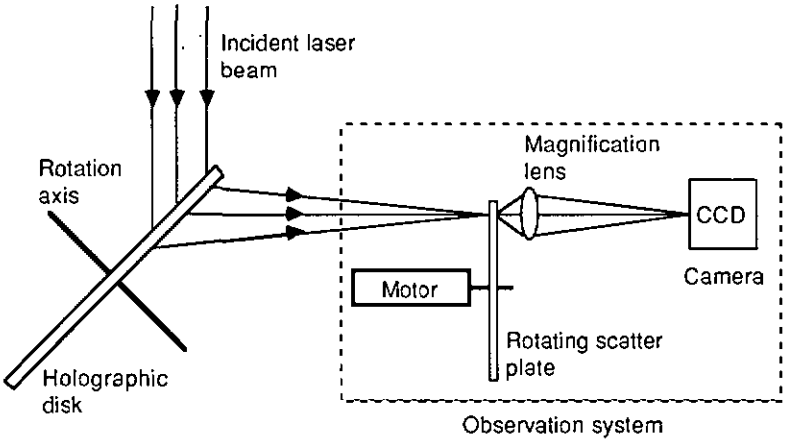

4.3 Experimental set-up for measuring the performances of the holographic scanners. The holographic disk rotates around its axis and generates a line perpendicular to the drawing plane. The observation system is translated along the generated line to determine the image point for different scan positions.

We determined the spot quality of the holographic scanning elements at different scan positions. Figure 4.3 shows the experimental set-up for measuring the image spot quality and its position with respect to a straight line. An incident laser beam is deflected by the holographic disk scanner and focussed on a scatter plate at the image plane. The holographic disk rotates around its axis and generates a scan line $\mathbf{y}(t)$ in the image plane; the scan line is perpendicular to the drawing plane. The observation system, also shown in the photograph in Fig.4.4, magnifies the image point and detects the spot quality with a CCD camera. Thus, it is possible to obtain the form as well as the profile of the spot simultaneously (Fig.4.5). To avoid the disturbing laser speckles, the scattering plate was rotated. During scanning, the observation system, including

the scatter plate, was translated parallel to the generated scan line. The scan line deviation Δy of the spot as a function of the scan length L was measured with the aid of a micrometer mounted on the observation system (Fig.4.4).

In our experiments, the scanning elements were segments of a disk, as shown in Fig.4.6. A complete holographic scanner would, of course, be a disk with several holograms, each generating its own line.

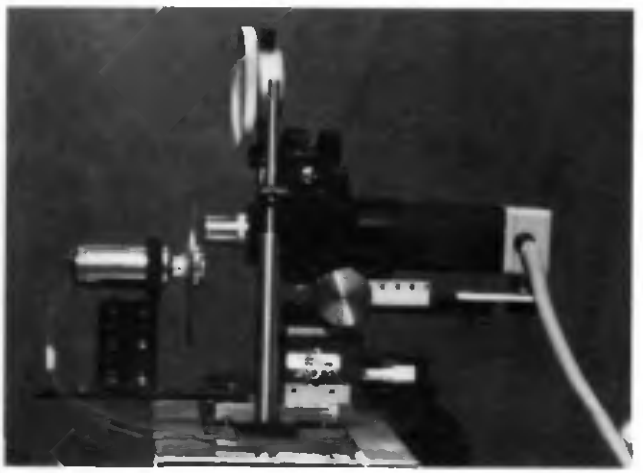

Fig.4.4. Observation system with a rotating scatter plate, microscope objective and CCD-camera. The vertical position of the system is measured with the aid of the micrometer.

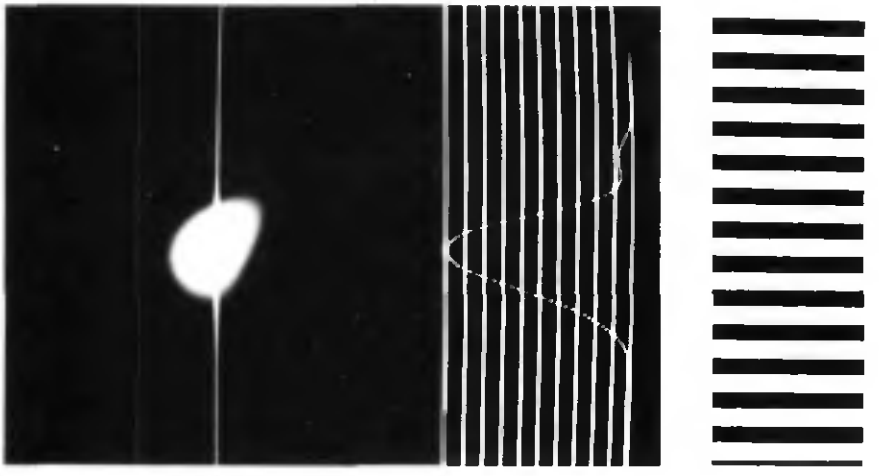

(a) (b)

Fig.4.5. a) Form and profile of an image point observed with the CCD-camera.
b) Scale: grating period ≡ 20 μm

Fig.4.6. Holographic disk.

4.3 Specific scanner configurations and results

Three disk configuration scanners were recorded, namely (I) uncorrected scanner, (II) straight-line scanner, (III) astigmatism-free scanner. Certain geometrical properties were identical for all three scanners: (a) symmetrical arrangement for the incident and outgoing beams ($\alpha = -\gamma$); (b) total deflection of about 90 deg ($|\alpha| + |\gamma|$); (c) scan length L = ±105 mm; (d) distance from the hologram to the scan line f = 300 mm; and (d) disk radius R = 40 mm. Also, the readout beam was a plane wave at the wavelength λ_r = 633 nm.

To distinguish the geometrical parameters ρ_R, f_R, α_R, γ_R , λ_R for recording, from the parameters ρ_r, f_r, α_r, γ_r, λ_r for reconstruction, we shall write them with an index. Note, that f_r is the distance from the hologram to the scan line, which is equal to the radius of the reconstructed object in the scan center (deflection angle $\beta = 0$).

4.3.1 Uncorrected scanner

The uncorrected scanner was realized by holographically recording the interference of a plane reference wave $\rho_R = \infty$ and a spherical object wave f_R = 300 mm. The recording wavelength λ_R was equal to the reconstructing wavelength λ_r = 633 nm, and the angles were $\alpha = -\gamma = 45.0$ deg for recording as well as for reconstruction.

The holographic disk was reconstructed with an incident plane wave at 45 deg, using the set-up shown in Fig.4.3. When rotating the disk around its axis, the focus point generated a scan line in the image plane. First, we determined the deviation Δy from a straight scan line. Figure 4.7 shows the experimental (+) and theoretical results (solid line). The calculations were performed using the ray tracing method, where the position of the focal spot in the image plane was assumed to be the center of gravity of the spot diagrams. As expected, the line generated by the uncorrected case I is strongly curved, ranging to ±500 μm. As shown, the experimental results follow closely the theoretical predictions.

Next we determined the spot quality for two different beam diameters D at various scan positions L = 0, ±30 mm, ±60 mm, +90 mm, ±105 mm in the

image plane. The experimental as well as the calculated results are shown in Fig.4.8 for D = 5 mm, and Fig.4.9 for D = 3 mm. In the scan center L = 0 mm, the generated spot is diffraction limited, because the recording and reconstruction parameters were identical. For a beam diameter of D = 5 mm, the spot diameter at half intensity is $D_S = \lambda f/D = 38$ µm (λ = 633 nm, f = 300mm) and for D = 3 mm, $D_S = \lambda f/D = 63$ µm. With an increasing scan length L the spot becomes strongly astigmatic, as shown for the experimental results as well as for the calculated spot diagrams. The strong aberrations are due to changes in geometry when the disk is rotated. In the case of a wavelength shift between recording and reconstruction, there would be additional aberrations, which would decrease the spot quality even in the scan center (L = 0 mm). To get improved results, the CGH must, therefore, compensate for the aberrations due to the disk rotation and the wavelength shift.

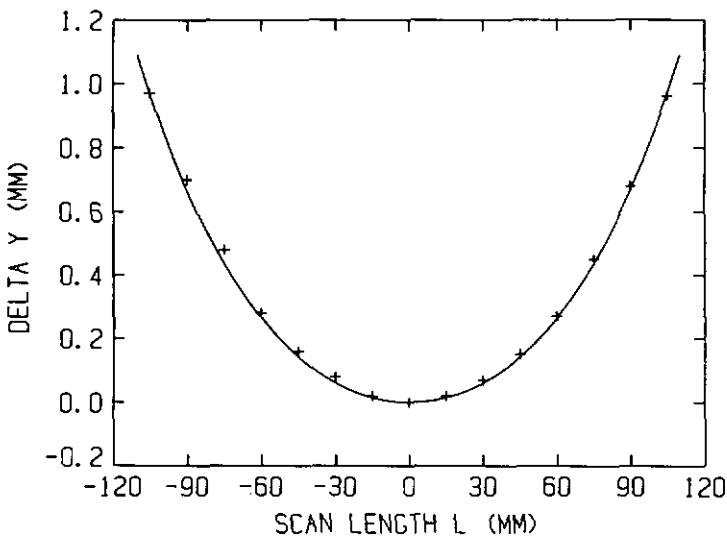

Fig.4.7. Calculated and measured deviation Δy of the scan from a straight line as a function of the scan length L for the uncorrected scanner. The maximum scan length was L = ± 105 mm. Calculated (solid line) is based on the center of gravity of the spots. Experimental (+).

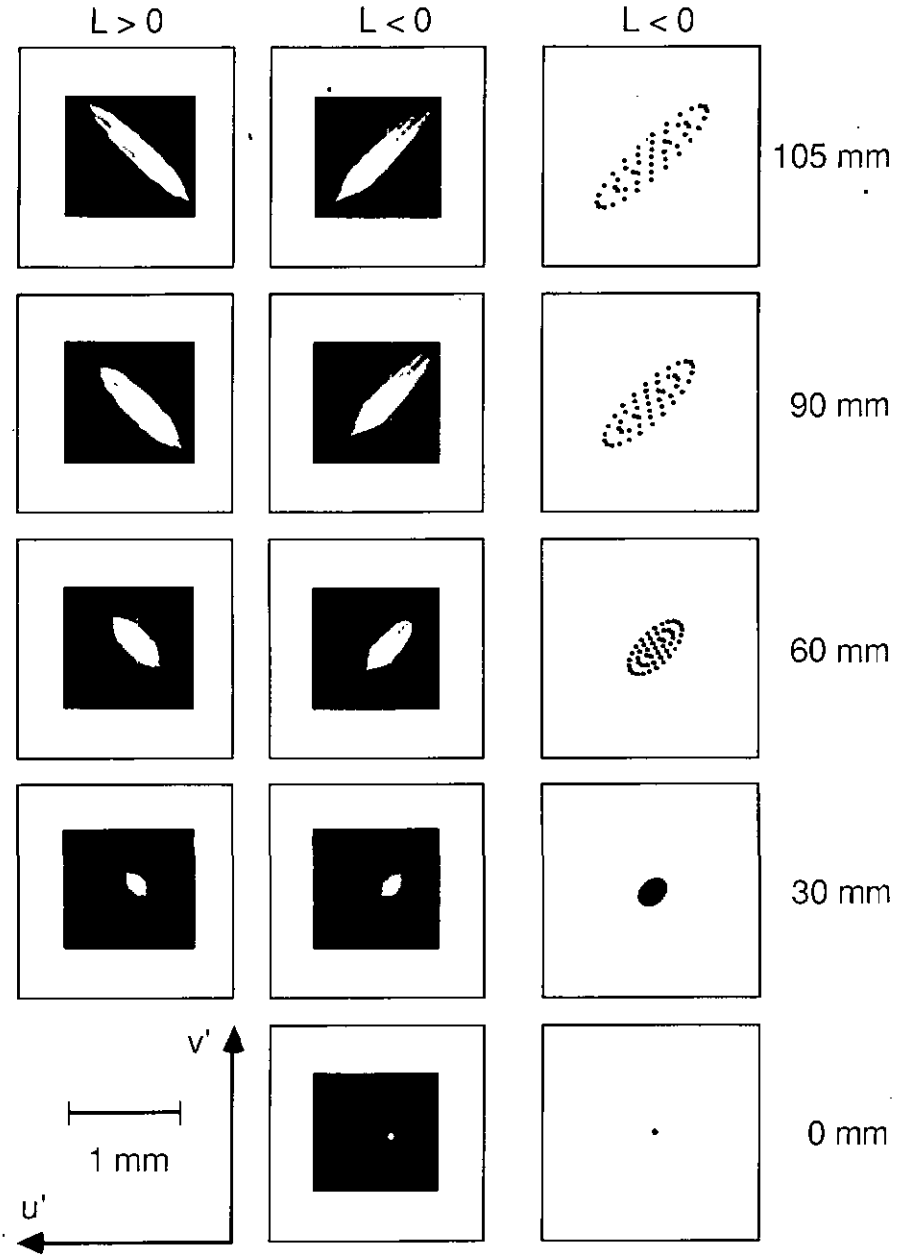

Fig.4.8. Spot quality for the uncorrected scanner with D = 5 mm (diffraction limited spot size D_S = 38 µm at half intensity). Experimental results and geometrical ray tracing for nine scan positions, corresponding to the scan lengths of L = 0, ± 30, ± 60, ± 90 and ± 105 mm. The scan line y(t) is parallel to u'-axis and the configuration is symmetrical with respect to the v'-axis.

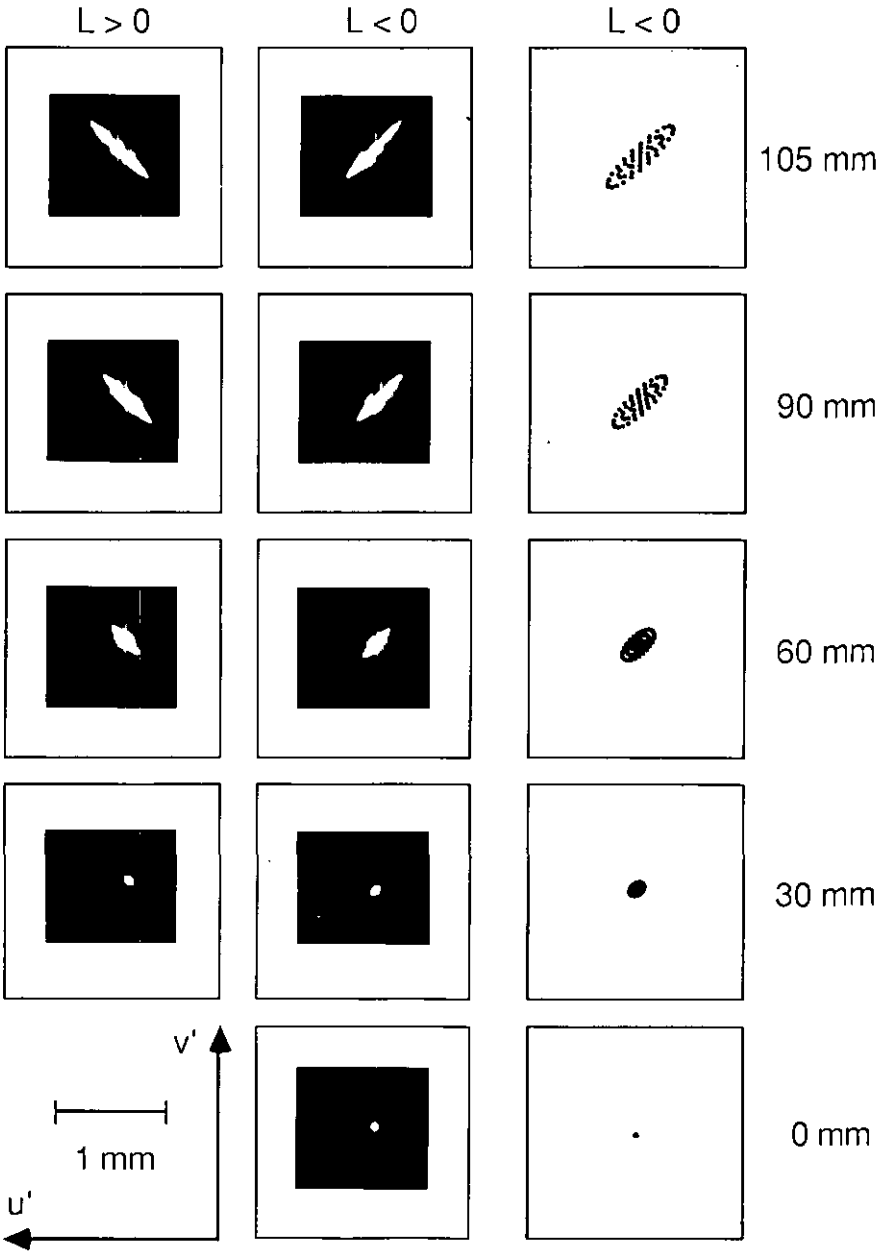

Fig.4.9. Spot quality for the uncorrected scanner with D = 3 mm (diffraction limited spot size D_S = 63 µm at half intensity). Experimental results and geometrical ray tracing for nine scan positions, corresponding to the scan lengths of L = 0, ± 30, ± 60, ± 90 and ± 105 mm. The scan line y(t) is parallel to u'-axis and the configuration is symmetrical with respect to the v'-axis.

4.3.2 Straight-line scanner

According to our analytical design method, the straight-line scanner, discussed in section 3.2.2, should be much better than the uncorrected scanner and should generate a straight line with minimized astigmatism of the focal spot (Fig.3.8). To test this prediction, we recorded and tested a straight-line scanner. For recording, the reference wave was an aspherical wave generated by a CGH, the object wave was a spherical wave with radius f_R = 428 mm and the angles were $\alpha_R = -\gamma_R = 34.5$ deg. The recording wavelength λ_R = 514 nm is now chosen to be different from the reconstructing wavelength λ_r = 633 nm. The geometrical parameters for reconstruction were $\rho_r = \infty$ (i.e. incident plane wave), and $\alpha_r = -\gamma_r = 44.15$ deg.

The calculated and experimental results are shown in Figs.4.10 - 4.12. Figure 4.10 shows the deviation Δy from a straight line as a function of the scan length L. Although, our design predicts a strictly straight line, there is some curvature. After closer scrutiny, we determined that indeed, the principle ray of the corrected scan moves strictly on a straight line; however, the center of gravity of the focal spot does not. The theoretical calculations for the center of gravity (solid line) were performed using the ray tracing method. The maximum deviation was found to be ±8 μm for a total scan length of L = ±105 mm, both for the experimental and theoretical results.

Next we determined the spot quality for two different beam diameters D at various scan positions L = 0, ±30 mm, ±60 mm, ±90 mm, ±105 mm in the image plane. The experimental as well as the calculated results are shown in Fig.4.11 for D = 5 mm, and Fig.4.12 for D = 3 mm. As shown, the spot size is significantly improved, when compared to the spots of the uncorrected scanner; note the different scales for the corrected and the uncorrected scanners. In Fig.4.11 we can see, that for a diameter of D = 5 mm a uniform scan is still not possible. The nearly diffraction limited spot size in the center (L = 0 mm) is much better than the spot at the end of the scan (L = ±105 mm). The decreasing quality can also be observed in the spot diagrams. The aberrations are much larger than the diffraction from the aperture. A smaller aperture increases the diffraction effect, but decreases the aberrations. This can be seen in Fig.4.12 from the experimental results, whereas the theoretical predictions only indicate the geometrical aberrations. For a diameter D = 3 mm, the

straight-line scanner generates a scan line with a good uniformity of the focal spot. The experimental spot size (diameter at half intensity) was found to be smaller than 85 μm for any position within the maximum scan length of L = ±105 mm.

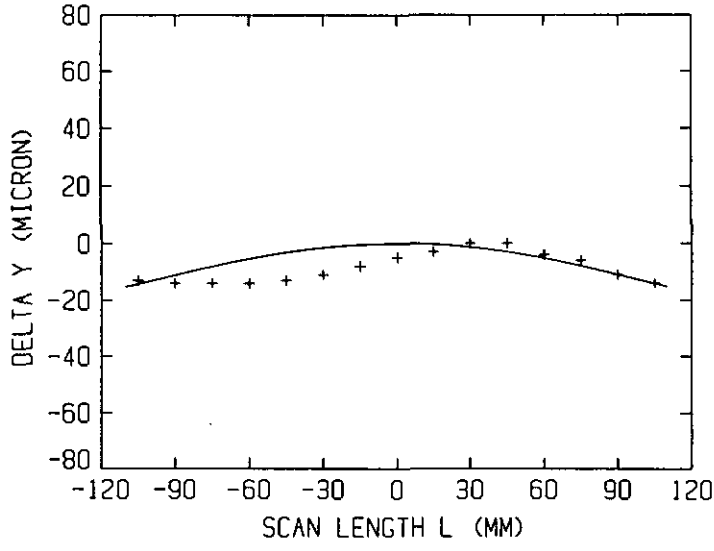

Fig.4.10. Calculated and measured deviation of the scan from a straight line Δy as a function of the scan length L for the straight-line scanner. The maximum scan length was L = ±105 mm. Calculated (solid line) is based on the center of gravity of the spots. Experimental (+).

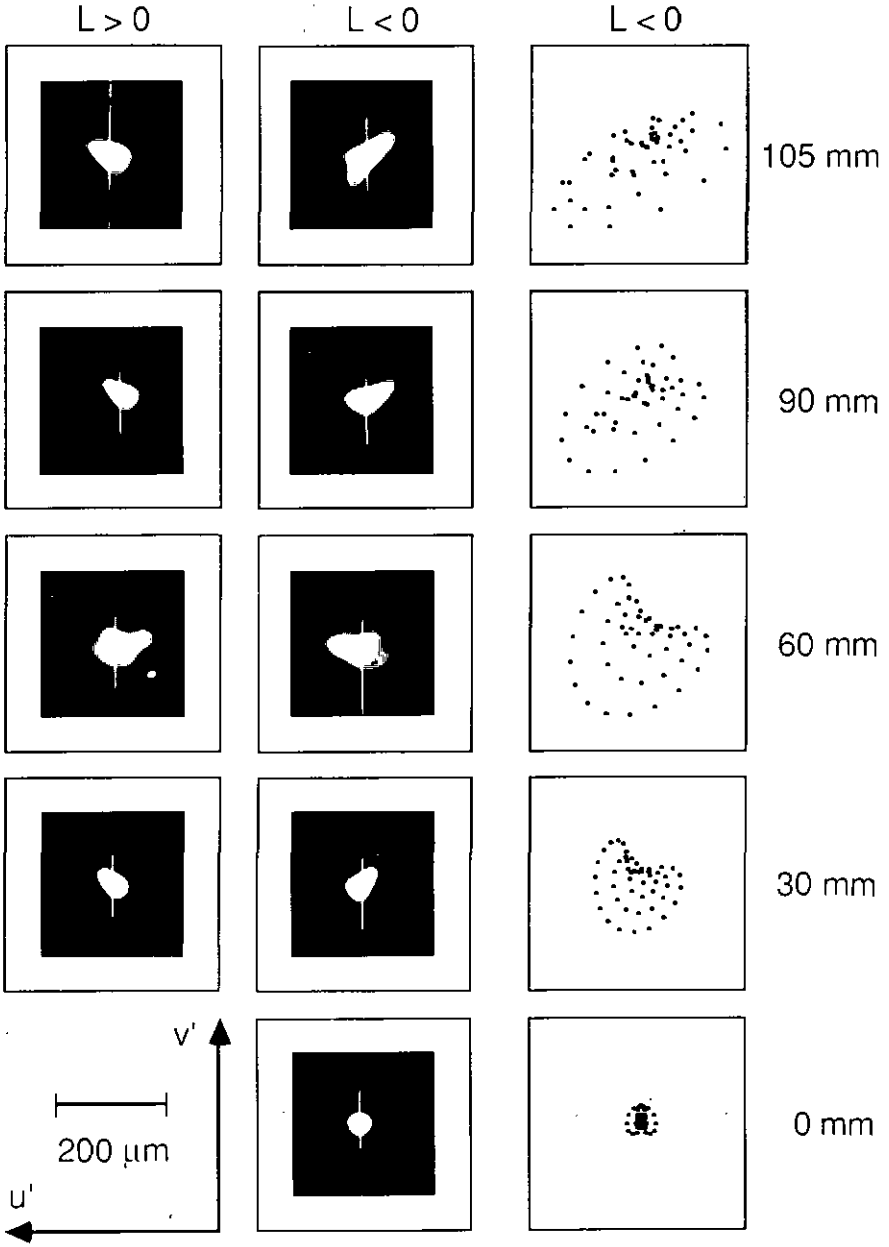

Fig.4.11. Spot quality for the straight-line scanner with D = 5 mm (diffraction limited spot size D_S = 38 µm at half intensity). Experimental results and geometrical ray tracing for nine scan positions, corresponding to the scan lengths of L = 0, ± 30, ± 60, ± 90 and ± 105 mm. The scan line y(t) is parallel to u'-axis and the configuration is symmetrical with respect to the v'-axis.

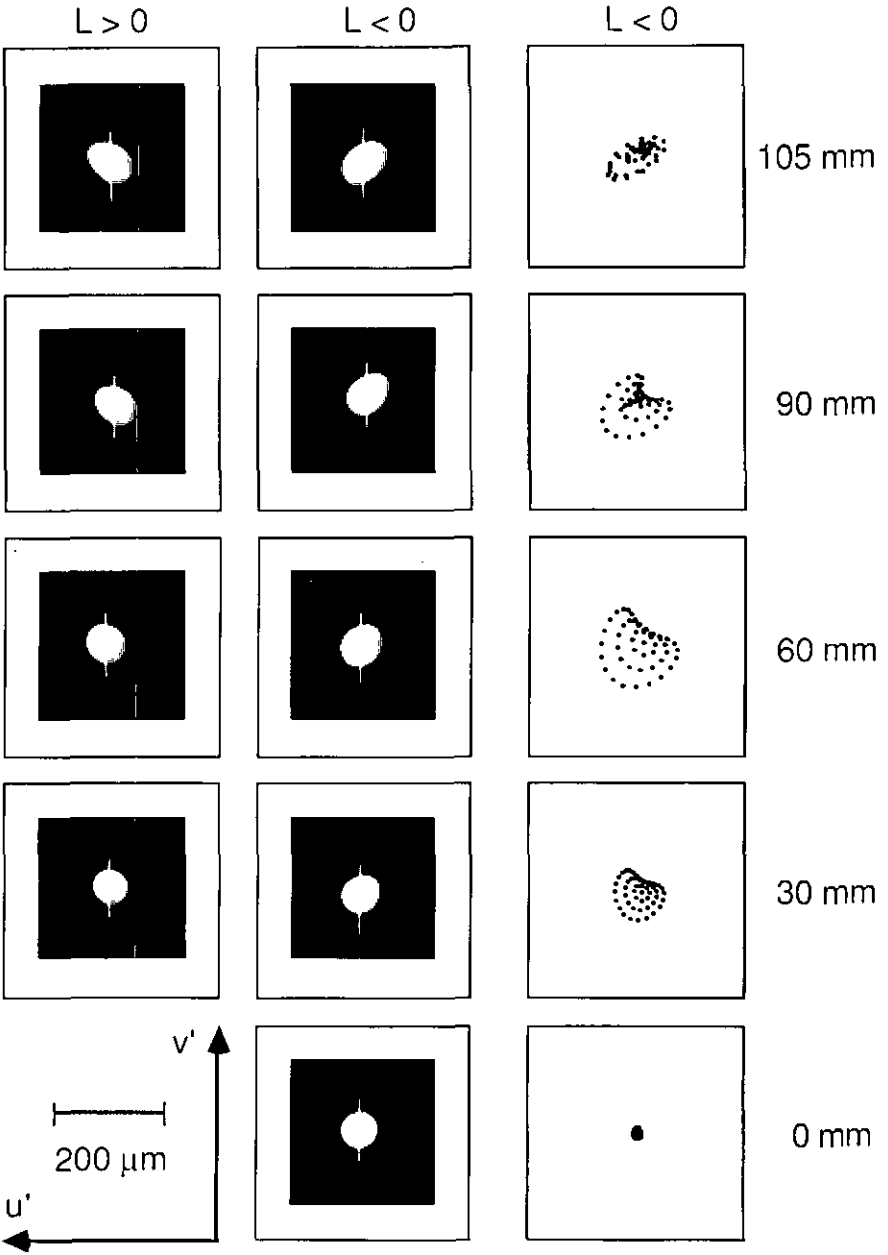

Fig.4.12. Spot qnality for the straight-line scanner with D = 3 mm (diffraction limited spot size D_S = 63 µm at half intensity). Experimental results and geometrical ray tracing for nine scan positions, corresponding to the scan lengths of L = 0, ± 30, ± 60, ± 90 and ± 105 mm. The scan line y(t) is parallel to u'-axis and the configuration is symmetrical with respect to the v'-axis.

4.3.3 Astigmatism-free scanner

Still better performance for the spot quality can be realized by a scanner which accepts a slightly curved scan line to compensate for the astigmatism of the outgoing wave. We recorded such a scanner, described in section 3.2.3 (Fig.3.14), according to our design method and then determined its behaviour. For recording, the reference wave was an aspherical wave, generated by a CGH, the object wave was spherical with a radius f_R = 430 mm and the angles were $\alpha_R = -\gamma_R = 34.81$ deg. The recording wavelength λ_R = 514 nm was again chosen differently from the reconstruction wavelength λ_r = 633 nm. For reconstruction, the incident beam was a plane wave $\rho_r = \infty$ and the angles $\alpha_r = -\gamma_r = 44.6$ deg.

The calculated and experimental results are shown in Figs.4.13 - 4.15. For this scanner a slightly curved scan line is expected. Figure 4.13 shows the deviation Δy from a straight line as a function of the scan length L for the experimental (+) and theoretical results (solid line). The calculations were performed using the ray tracing method, where the position of the focal spot in the image plane was assumed to be the center of gravity of the spot diagrams. We found, that the scan line is slightly curved, within ±30 µm around a center line, for a total scan length of L = ±105 mm, as it was predicted by the theoretical calculations.

Next, we determined the spot quality for two different beam diameters D at various scan positions L = 0, ±30 mm, ±60 mm, ±90 mm, ±105 mm in the image plane. The experimental as well as the calculated results are shown in Fig.4.14 for D = 5 mm, and Fig.4.15 for D = 3 mm. From the ray tracing results, the spot quality is expected to be still better than in the case of a straight-line scanner. This is in fact so, comparing the results shown in Fig.4.14 (astigmatism-free scanner) with Fig.4.11 (straight-line scanner). Already for a diameter of D = 5 mm the spot has a good uniformity during scanning, where the experimental spot size (diameter at half intensity) was found to be smaller than 60 µm for any position within the maximum scan length of L = ±105 mm. As shown in the results of Fig.4.15 the maximum spot diameter becomes larger for a beam diameter D = 3 mm. Consequently, it is not useful to work with a smaller aperture, because the aperture diffraction effect is now more influential than the reduction of the aberrations.

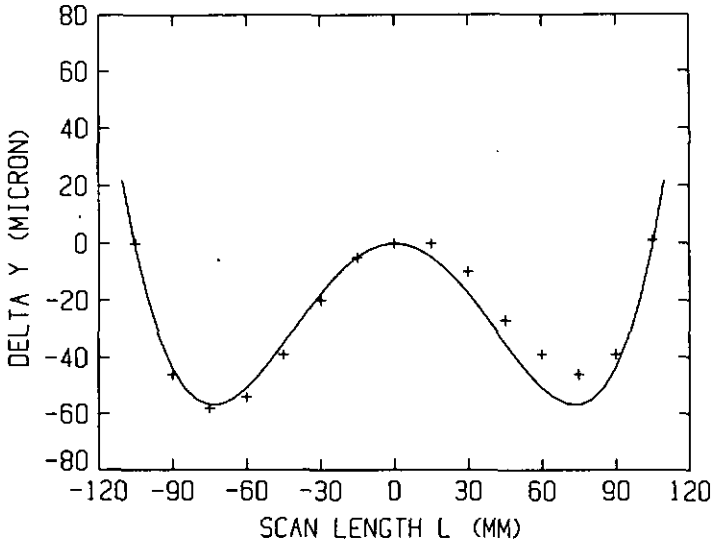

Fig.4.13. Calculated and measured deviation Δy of the scan from a straight line as a function of the scan length L for the astigmatism-free scanner. The maximum scan length was L = ± 105 mm. Calculated (solid line) is based on the center of gravity of the spots. Experimental (+).

4.3.4 Concluding remarks

Three symmetrical disk configuration scanners reconstructed with plane incident beams were evaluated. The uncorrected scanner showed strong aberrations even without a wavelength shift between recording and reconstruction, and is deemed impractical for most applications. Improved results were obtained for scanners, which were recorded with the aid of CGHs according to our design methods. These improved results were obtained also when the recording wavelength λ_R was different from the reconstruction wavelength λ_r. Specifically, for the straight-line scanner, the experimental spot diameters (at half intensity) for a scan length of L = ±105 mm and an image plane distance of f = 300 mm were found to be less than 85 μm for a maximum deviation of the straight line of ±8 μm, whereas for the astigmatism-free scanner the spot diameters were less than 60 μm for a maximum deviation of ±30 μm. The choice for selecting one scanner design over the other depends on the specific requirements for the scanners.

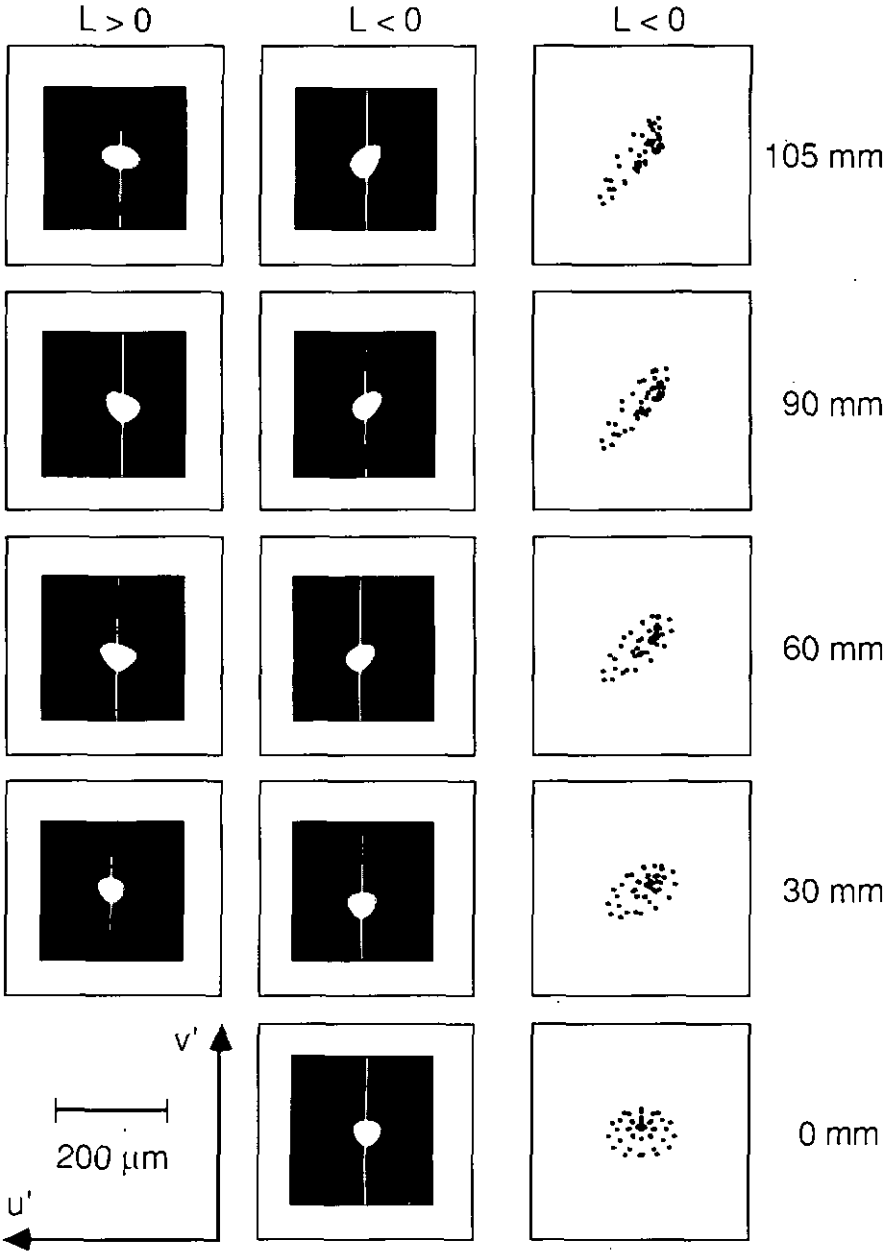

Fig.4.14. Spot quality for the astigmatism-free scanner with D = 5 mm (diffraction limited spot size D_S = 38 µm at half intensity). Experimental results and geometrical ray tracing for nine scan positions, corresponding to the scan lengths of L = 0, ± 30, ± 60, ± 90 and ± 105 mm. The scan line y(t) is parallel to u'-axis and the configuration is symmetrical with respect to the v'-axis.

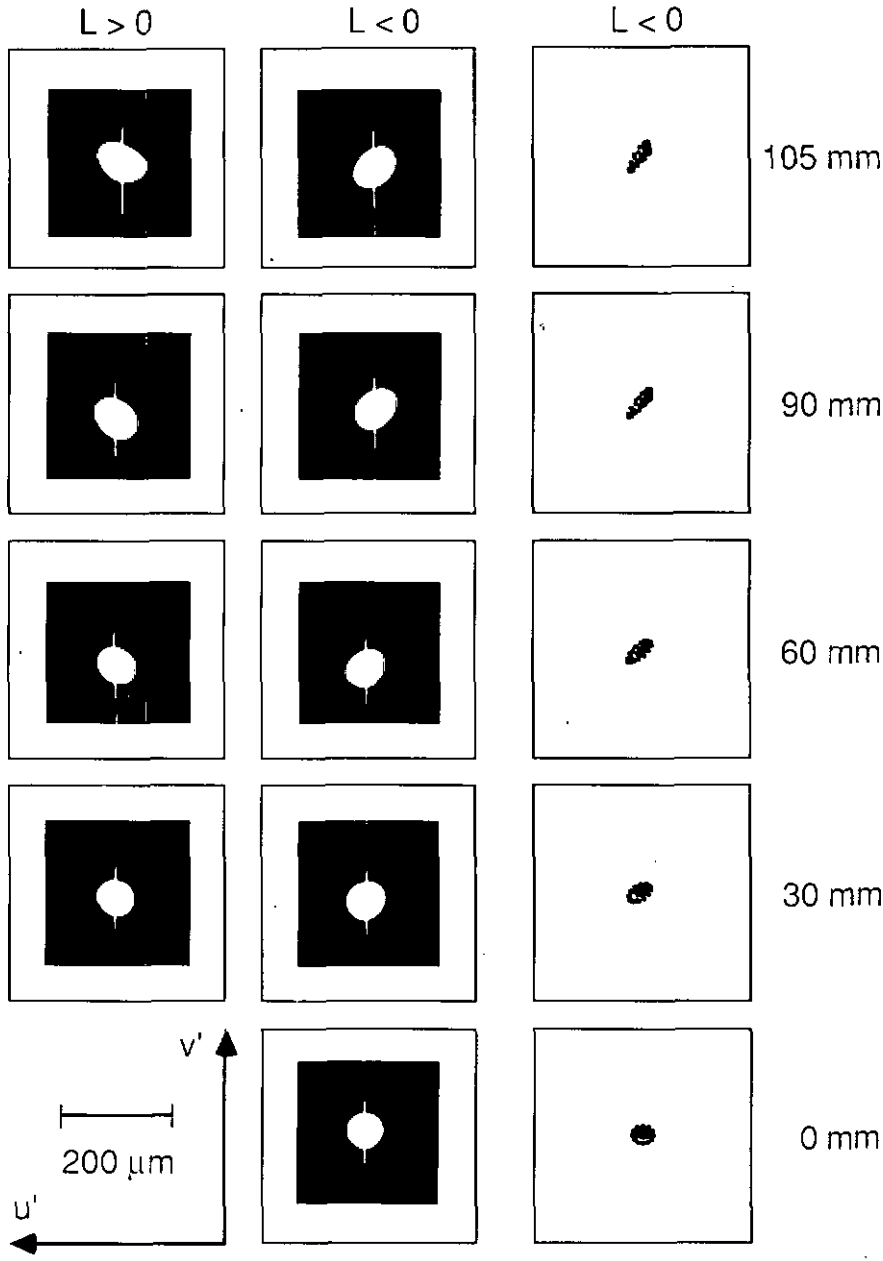

Fig.4.15. Spot quality for the astigmatism-free scanner with D = 3 mm (diffraction limited spot size D_S = 63 µm at half intensity). Experimental results and geometrical ray tracing for nine scan positions, corresponding to the scan lengths of L = 0, ± 30, ± 60, ± 90 and ± 105 mm. The scan line y(t) is parallel to u'-axis and the configuration is symmetrical with respect to the v'-axis.

5. HIGHER ORDER ABERRATIONS

In the preceding chapters the phase function of holographic scanners were found by using second order approximation for the incident and outgoing beams. We shall now consider, whether it is possible to further improve the scanner design by using also third or fourth order terms to describe the beams. We shall begin by extending the second order theory to higher order in a general manner, and then, to avoid overly cumbersome formulas, we shall present a simplified method. Finally, we shall apply the simplified method for designing disk configuration scanners.

5.1 General phase function

To extend the second order theory up to n-th order, additional derivatives of the local hologram phase function $\Psi(u,v,t)$ [$h_i(t)$, $h_{ij}(t)$, ..., in Eqs.(2.5) and(2.6)] have to be calculated. To do so, we follow the procedure outlined in section 2.3. First a general optical phase $\Phi(\mathbf{X})$ is developed up to n-th order around the propagation axis given by the wave vector $\mathbf{k}$ [Eq.(2.17)]. We assume, that the phase is known in the X,Y-plane [Fig.2.3], which is perpendicular to $\mathbf{k}$. To calculate the phase $\Phi(u,v)$, where the uv-plane (hologram plane) is usually different from the X,Y-plane, the propagation of Φ in the Z-direction, namely $\Phi(X,Y,Z)$, must first be determined. As the beam waist is large compared with the wavelength, the eikonal equation ([26], p.112) is valid in this region for describing the propagation. Once $\Phi(X,Y,Z)$ is known, a coordinate transformation from the X,Y,Z-system to the u,v,w-system yields the local phase $\Phi(u,v,w=0)$ in the hologram plane. Now, from this local phase it is possible to obtain the incident $\Phi_r(u,v)$ and the outgoing beams $\Phi_P(u,v,t)$ as general phases; the outgoing beams represent a continuous set of waves focussed on the scan line $\mathbf{y}(t)$. Finally, the local hologram phase $\Psi(u,v,t)$ is obtained from the condition of phase matching [Eq.(2.24)].

We shall now consider the steps necessary to obtain the derivatives of the local phase Ψ, the functions $h_{i..j}(t)$. We begin by describing a general wave up to the n-th order, where the optical phase function $\Phi(\mathbf{X})$ is developed in a Taylor series, namely

$$\Phi(\mathbf{X}) = \Phi_0 + \frac{\partial \Phi}{\partial X_i} X_i + \frac{1}{2} \frac{\partial^2 \Phi}{\partial X_i \partial X_j} X_i X_j + \frac{1}{6} \frac{\partial^3 \Phi}{\partial X_i \partial X_j \partial X_k} X_i X_j X_k + \ldots . \qquad (5.1)$$

with i,j,k = 1,2,3, where (X,Y,Z) = (X_1,X_2,X_3). We assume, that the phase function Φ is given up to fourth order in the X,Y-plane and the Z-axis is parallel to the direction of propagation. Since there is no symmetry, all coefficients must exist. Equation 5.1 thus becomes

$$\begin{aligned} \Phi(X,Y,Z=0) = \Phi_0 + k\,[&(1/2)(A_{20}X^2 + 2\,A_{11}\,XY + A_{02}\,Y^2) \\ &+ (1/6)(\,C_{30}\,X^3 + 3\,C_{21}\,X^2Y + 3\,C_{12}\,XY^2 + C_{03}\,Y^3) \\ &+ (1/24)(\,S_{40}\,X^4 + 4\,S_{31}\,X^3Y + 6\,S_{22}\,X^2Y^2 + 4\,S_{13}\,XY^3 + S_{04}Y^4)], \end{aligned} \qquad (5.2)$$

where the notation

$$\frac{\partial^{(l+m+n)}\Phi}{\partial X^l \partial Y^m \partial Z^n} \equiv S_{lmn} \qquad (5.3)$$

is used for the coefficients of $X^lY^mZ^n$. Also, A stands for the second order (l+m+n = 2), C for the third order and S for the fourth order coefficients. If n is equal to zero, only S_{lm} is written. All derivatives are given at the origin (X=Y=Z=0). Recall that in section 2.3 we defined $\partial^2\Phi/\partial X^2 = a$, $\partial^2\Phi/\partial Y^2 = b$ and $\partial^2\Phi/\partial X\partial Y = e$.

The coefficients A_{ijk}, C_{ijk}, S_{ijk}, describing the propagation in the Z-direction, are given by the coefficients of the phase in the X,Y-plane and by the propagation. As mentioned above, the eikonal equation determines the condition for propagation, which means

$$(\mathrm{grad}\phi(\mathbf{X}))^2 = n^2(\mathbf{X}). \qquad (5.4)$$

The function ϕ represents the optical path length, also called the eikonal, and n the refractive index. The optical phase Φ and the path length ϕ are related by $\Phi = k\,\phi$. The eikonal equation (5.4) can now be written differently as

$$(\mathrm{grad}\Phi(\mathbf{X}))^2 = k^2\,n^2(\mathbf{X}). \qquad (5.5)$$

where $k = 2\pi/\lambda$ and in our case $n(\mathbf{X}) = 1$. Because the Z-axis is chosen to be parallel to the direction of propagation, we get

$$\frac{\partial \Phi}{\partial X} = 0, \qquad \frac{\partial \Phi}{\partial Y} = 0, \qquad \frac{\partial \Phi}{\partial Z} = k, \tag{5.6}$$

Introducing the phase Φ (Eq.5.1) into the eikonal equation (5.5), yields for the coefficients equal to zero

$$\frac{\partial^2 \Phi}{\partial X \partial Z} = A_{101} = 0, \qquad \frac{\partial^2 \Phi}{\partial Y \partial Z} = A_{011} = 0, \qquad \frac{\partial^2 \Phi}{\partial Z^2} = A_{002} = 0,$$

$$\frac{\partial^3 \Phi}{\partial X \partial Z^2} = C_{102} = 0, \qquad \frac{\partial^3 \Phi}{\partial Y \partial Z^2} = C_{012} = 0, \qquad \frac{\partial^3 \Phi}{\partial Z^3} = C_{003} = 0, \tag{5.7}$$

$$\frac{\partial^4 \Phi}{\partial X \partial Z^3} = S_{103} = 0, \qquad \frac{\partial^4 \Phi}{\partial Y \partial Z^3} = S_{013} = 0, \qquad \frac{\partial^4 \Phi}{\partial Z^4} = S_{004} = 0,$$

and for the coefficients different from zero

$$C_{201} = -\,(A_{20}^2 + A_{11}^2),$$

$$C_{111} = -\,A_{11}\,(A_{20} + A_{02}),$$

$$C_{021} = -\,(A_{11}^2 + A_{02}^2),$$

$$S_{301} = -\,3\,(A_{20}\,C_{30} + A_{11}\,C_{21}),$$

$$S_{211} = -\,C_{21}\,(2\,A_{20} + A_{02}) - A_{11}\,(2\,C_{12} + C_{30}), \tag{5.8}$$

$$S_{202} = 2\,(A_{20}^3 + 2\,A_{20}\,A_{11}^2 + A_{11}^2\,A_{02}),$$

$$S_{121} = -\,C_{12}\,(A_{20} + 2\,A_{02}) - A_{11}\,(2\,C_{21} + C_{03}),$$

$$S_{112} = 2\,A_{11}\,(A_{20}^2 + 2\,A_{20}\,A_{02} + A_{02}^2 + A_{11}^2),$$

$$S_{031} = -\,3\,(A_{11}\,C_{12} + A_{02}\,C_{03}),$$

$$S_{022} = 2\,(A_{11}^2\,A_{20} + 2\,A_{11}^2\,A_{02} + A_{02}^3).$$

The phase function $\Phi(\mathbf{X})$ can now be represented completely by the phase in the X,Y plane $\Phi(X,Y,Z=0)$ [Eq.(5.2)] and the propagation terms C_{ijk}, S_{ijk} [Eq.(5.8)], namely

$$\begin{aligned}\Phi(X,Y,Z) = \Phi(X,Y,Z=0) + k\,[Z + (1/6)(3\,C_{201}\,X^2Z + 6\,C_{111}\,XYZ + 3\,C_{021}\,Y^2Z) \\ + (1/24)(4\,S_{301}\,X^3Z + 12\,S_{211}\,X^2YZ + 6\,S_{202}\,X^2Z^2 \\ +12\,S_{121}\,XY^2Z + 12\,S_{112}\,XYZ^2 + 4\,S_{031}\,Y^3Z + 6\,S_{022}\,Y^2Z^2)].\end{aligned} \tag{5.9}$$

The phase in the hologram plane $\Psi(u,v,t)$ is essentially governed by the condition of phase matching, which is

$$\Psi(\mathbf{u}_H,t) = \Phi_p(\mathbf{u}_H,t) - \Phi_r(\mathbf{u}_H), \tag{5.10}$$

where r means the reconstructing beam and P the reconstructed wave front, focussed on the line $\mathbf{y}(t)$. The phase distributions for each wave in the hologram plane has to be calculated first. The geometrical relation of the hologram plane u,v,w=0 and the X,Y,Z-coordinate system of the waves is sketched in Fig.2.3. The direction of propagation is given by two angles α, β, for the outgoing wave and γ, δ, for the incident wave. The transformation from the (X,Y,Z) to the (u,v,w) coordinates is performed by two rotations in sequence. The first around the Y-axis by the angle β (δ respectively) and the second around the u-axis by the angle α (γ respectively). The corresponding transformation matrix is given in Eq.(2.26).

The calculations proceed along the same line as in section 2.3. The derivatives of the local phase function $\Psi(u,v,t)$, i.e. $h_{ijk}(t)$ in Eqs.(2.5) and (2.6) have to be established. For a spherical incident wave with the curvature $1/\rho$ and the angles γ and δ ($\delta = 0$), the derivatives are

$$h_1 = k \sin\beta, \qquad h_2 = k\,(\sin\alpha \cos\beta - \sin\gamma),$$

$$h_{11} = k\,(A_{20} \cos^2\beta - 1/\rho),$$

$$h_{12} = k\,[\cos\beta\,(A_{11} \cos\alpha - A_{20} \sin\alpha \sin\beta)],$$

$$h_{22} = k\,(A_{20}\sin^2\alpha \sin^2\beta - 2\,A_{11} \sin\alpha \cos\alpha \sin\beta + A_{02} \cos^2\alpha - \cos^2\gamma/\rho),$$

$$h_{111} = k\,[C_{30}\,\cos^3\beta - 3\,(A_{20}^2 + A_{11}^2)\,\sin\beta\,\cos^2\beta],$$

(5.11)

$$\begin{aligned} h_{112} = k\,[&- C_{30}\,\sin\alpha\,\sin\beta\,\cos^2\beta + C_{21}\,\cos^2\beta\,\cos\alpha + \sin\gamma/\rho^2 \\ &- (A_{20}^2 + A_{11}^2)\,(\sin\alpha\,\cos^3\beta - 2\,\sin\alpha\,\sin^2\beta\,\cos\beta) \\ &- 2\,A_{11}(A_{20} + A_{02})\,\cos\alpha\,\sin\beta\,\cos\beta], \end{aligned}$$

$$\begin{aligned} h_{122} = k\,[&C_{30}\,\cos\beta\,\sin^2\alpha\,\sin^2\beta - 2\,C_{21}\,\sin\alpha\,\cos\alpha\,\sin\beta\,\cos\beta + C_{12}\,\cos^2\alpha\,\cos\beta \\ &- (A_{20}^2 + A_{11}^2)(\sin^2\alpha\,\sin^3\beta - 2\,\sin^2\alpha\,\cos^2\beta\,\sin\beta) \\ &- 2\,A_{11}(A_{20} + A_{02})\,(\sin\alpha\,\cos\alpha\,\cos^2\beta - \sin\alpha\,\cos\alpha\,\sin^2\beta) \\ &- (A_{11}^2 + A_{02}^2)\,(\cos^2\alpha\,\sin\beta)], \end{aligned}$$

$$\begin{aligned} h_{222} = k\,[&- C_{30}\,\sin^3\alpha\,\sin^3\beta + 3\,C_{21}\,\sin^2\alpha\,\cos\alpha\,\sin^2\beta - 3\,C_{12}\,\sin\alpha\,\cos^2\alpha\,\sin\beta \\ &+ C_{03}\,\cos^3\alpha - 3(A_{20}^2 + A_{11}^2)\,\sin^3\alpha\,\sin^2\beta\,\cos\beta \\ &+ 6\,A_{11}(A_{20} + A_{02})\,\sin^2\alpha\,\cos\alpha\,\sin\beta\,\cos\beta \\ &- 3(A_{11}^2 + A_{02}^2)\,\sin\alpha\,\cos^2\alpha\,\cos\beta + 3\,\sin\gamma\,\cos^2\gamma/\rho^2], \end{aligned}$$

with $h_{ijk} = h_{ikj} = h_{kij} = \ldots$

The functions $h_{ijk}(t)$ are the derivatives of the local phase function $\Psi(u,v,t)$, defined as

$$\frac{\partial^3\Psi}{\partial u_i \partial u_j \partial u_k} \equiv h_{ijk}, \qquad i,j,k = 1,2, \tag{5.12}$$

and similarly for the first and the second derivatives h_i and h_{ij}. Note that for non-planar holograms, the w-coordinate is also necessary (i.e. i,j,k = 1,2,3) because the hologram is no longer in the u,v-plane.

The expressions h_{ijk} up to third order are already cumbersome and become even worse for fourth order. Although it is possible to proceed with the calculations, the interpretation of the resulting formulas will be difficult.

An alternative technique, in which the wavefronts are analyzed by the principle of the error function, is more promising for investigating higher order aberrations, as will be shown in the following section.

5.2 The principle of the error function

A general scan geometry is assumed as sketched in Fig.2.1, where a laser beam is deflected and focussed by a holographic optical element (HOE). The hologram structure can be described by a phase function $\Phi(x,y)$. While displacing the HOE, the incident beam moves along a line $\mathbf{x}(s)$ in the hologram plane and the image point describes another line $\mathbf{y}(t)$ in space. As done in chapter 2, a local coordinate system u,v,w is introduced, so that the w-axis is normal to the hologram plane. During the scan motion, the origin of the system u,v,w is at the center of the incident laser beam and on the line $\mathbf{x}(s)$ in the hologram plane. Now, we describe the hologram reconstruction in the local coordinate system u,v as

$$\Phi_r(u,v) + \Phi(u,v,s) = \Phi_p(u,v,t) = \Phi_i(u,v,t) + F(u,v,t). \qquad (5.13)$$

The readout beam $\Phi_r(u,v)$ (plane or spherical wave) illuminates the hologram $\Phi(u,v,s)$ at $\mathbf{x}(s)$ and generates an outgoing wave $\Phi_p(u,v,t)$, focussed onto the scan line $\mathbf{y}(t)$. As known from the previous chapters, the outgoing wave is usually not ideally spherical. Thus, it can be represented as a spherical wave $\Phi_i(u,v,t)$ plus an error function $F(u,v,t)$. Since now all waves, except for the error $F(u,v,t)$, are spherical, the analysis becomes simpler than in section 5.1. It should be noted that the error function contains all the aberrations which are no longer easy separable.

During scanning, the hologram phase function $\Phi(u,v,s)$ changes with the parameter s, which describes the position of the readout beam on $\mathbf{x}(s)$ in the hologram plane. The outgoing wave $\Phi_p(u,v,t)$ changes with the parameter t, which describes the position of the focus on the generated line $\mathbf{y}(t)$ in space. The relation between s and t is not a priori known. The difference between the outgoing wave and the reconstructing wave in the hologram plane as a function of t [Eq.(5.13)] can be described by a function $\Psi(u,v,t)$, namely

$$\Psi(u,v,t) \equiv \Phi_p(u,v,t) - \Phi_r(u,v) = \Phi_i(u,v,t) + F(u,v,t) - \Phi_r(u,v). \qquad (5.14)$$

The calculations proceed now along the same lines as in section 2.1. First, the two phase functions $\Phi(u,v,s)$ and $\Psi(u,v,t)$ are both expanded in Taylor series about the point $\mathbf{x}(s)$ [Eqs.(2.2) and (2.3)]. Then, to get a local match, we require

that the two series are equal up to the n-th order [Eqs.(2.5) and (2.6)]. Finally, to determine the hologram phase function $\Phi(x,y)$, where x,y are the hologram coordinates (Fig.2.1), the relations between the derivatives of the two coordinate systems x,y and u,v have to be established [Eqs.(2.7) and (2.8)]. This yields the relations between the derivatives of the hologram phase function $\Phi(x,y)$ and the derivatives of the local phase function $\Psi(u,v,t)$, i.e. the functions $h_{1..j}(t)$ [Eqs.(2.9) and (2.10)].

To calculate the derivatives of the local phase function $\Psi(u,v,t)$ at the point $\mathbf{x}(s)$, it is necessary to determine first the phases of the spherical waves $\Phi_i(u,v,t)$ and $\Phi_r(u,v)$. Following Figs.2.1 and 2.3, the spherical wave Φ_i is given by

$$\Phi_i(u,v,t) = k\,[(u + \sin\beta/a)^2 + (v + \sin\alpha\cos\beta/a)^2 + (\cos\alpha\cos\beta/a)^2]^{1/2}. \qquad (5.15a)$$

Since Φ_i is assumed to be ideally focussed onto the scan line $\mathbf{y}(t)$, the directions $\alpha(t)$ and $\beta(t)$ and the curvature a(t) are completely determined by the scan geometry. Note that a(t) is negative for a convergent wave. Similarly, the readout beam is given by

$$\Phi_r(u,v,t) = k\,[(u)^2 + (v + \rho\sin\gamma)^2 + (\rho\cos\gamma)^2)^{1/2}, \qquad (5.15b)$$

where γ is the inclination with respect to the hologram normal and ρ is the radius of curvature.

Now, we get from Eq.(5.14) for the functions $h_{1..j}(t) \equiv \partial^m\Psi(u,v,t)/\partial u_1..\partial u_j$

$$h_1 = \sin\beta + F_1\,. \qquad (5.16a)$$

$$h_2 = \sin\alpha\cos\beta - \sin\gamma + F_2\,. \qquad b)$$

$$h_{11} = a\cos^2\beta - 1/\rho + F_{11}. \qquad c)$$

$$h_{12} = -\,a\sin\alpha\sin\beta\cos\beta + F_{12}\,. \qquad d)$$

$$h_{22} = a\,(1 - \sin^2\alpha\cos^2\beta) - \cos^2\gamma/\rho + F_{22}\,. \qquad e)$$

$$h_{111} = -\,3\,a^2\sin\beta\cos^2\beta + F_{111}\,. \qquad f)$$

$$h_{112} = a^2 \sin\alpha \cos\beta\,(3\sin^2\beta - 1) + \sin\gamma/\rho^2 + F_{112}\,. \qquad g)$$

$$h_{122} = a^2 \sin\beta\,(3\sin^2\alpha\cos^2\beta - 1) + F_{122}\,. \qquad h)$$

$$h_{222} = 3\,a^2 \sin\alpha\cos\beta\,(\sin^2\alpha\cos^2\beta - 1) + 3\sin\gamma\cos^2\gamma/\rho^2 + F_{222}\,. \qquad i)$$

$$h_{1111} = 3\,a^3\,(-1 + 6\sin^2\beta - 5\sin^4\beta) + 3/\rho^3 + F_{1111}. \qquad k)$$

$$h_{1112} = 3\,a^3\,(\sin\alpha\sin\beta\cos\beta\,(3 - 5\sin^2\beta) + F_{1112}\,. \qquad l)$$

$$h_{1122} = a^3\,(-1 + 3\sin^2\alpha\cos^2\beta + 3\sin^2\beta - 15\sin^2\alpha\sin^2\beta\cos^2\beta) + (1 - 3\sin^2\gamma)/\rho^3 + F_{1122}\,. \qquad m)$$

$$h_{1222} = 3\,a^3\sin\alpha\sin\beta\cos\beta\,(3 - 5\sin^2\alpha\cos^2\beta) + F_{1222}\,. \qquad n)$$

$$h_{2222} = 3\,a^3\,(-1 + 6\sin^2\alpha\cos^2\beta - 5\sin^4\alpha\cos^4\beta) + 3\,(1 - 6\sin^2\gamma + 5\sin^4\gamma)/\rho^3 + F_{2222}\,. \qquad o)$$

where $F_{i..j}(t) \equiv \partial^n F(u,v,t)/\partial u_i..\partial u_j$.

Next, the local derivatives of $\Phi(u,v,s)$ have to be calculated and matched with the above $h_{i..j}$. For this purpose, we consider a particular geometry, namely a disk configuration scanner generating a straight line in space.

5.3 Higher order analysis for disk configuration scanners

The principle of the error function is now applied to a disk configuration scanner. The geometrical arrangement is shown in Fig.3.3, where the polar coordinates r,ϕ are the hologram coordinates. The line $\mathbf{x}(s)$ is a circle of radius R, i.e. $\phi(s) = \phi$, $r(s) = R$. Similar to Eq.(3.17), we assume for the phase function $\Phi(r,\phi)$ a fourth order approximation perpendicular to the scan line, namely

$$\Phi(r,\phi) = k\,[a_0 + a_1(r-R) + \frac{1}{2}\,a_2(r-R)^2 + \frac{1}{6}\,a_3(r-R)^3 + \frac{1}{24}\,a_4(r-R)^4]. \qquad (5.17)$$

where $a_k = a_k(\phi)$.

The incident beam is a spherical wave with a radius of curvature ρ and inclined at an angle γ. As shown in Fig.3.3. the generated line $\mathbf{y}(t)$ should be a straight line in space. Therefore, the deflection angle $\beta(t)$ is chosen to be equal to the scan parameter t ($\beta = t$), the inclination $\alpha(\beta)$ is constant ($\alpha = \alpha_c$), and the curvature $a(\beta)$ is determined by the focussing condition $a(\beta) = -\cos\beta/f$.

To determine the functions $a_k(\phi)$, we proceed as shown in section 2.1 in general, and in section 3.2 for disk configuration scanners in detail. First, the relations of the hologram coordinates r,ϕ and the local coordinates have to be established [Eqs.(2.7) and (2.8)]. Then the derivatives of the hologram phase function $\Phi(x,y)$ [Eq.(5.17)] and the derivatives of the functions $\Psi(u,v,t)$, i.e. $h_{l..j}(t)$ in Eqs.5.16) have to be matched along $\mathbf{x}(s)$ [Eqs.2.9 and 2.10]. This yields finally

$$F_1 = a_0'/R - \sin\beta, \tag{5.18a}$$

$$F_2 = a_1 - \sin\alpha\cos\beta + \sin\gamma, \tag{b}$$

$$F_{11} = a_0''/R^2 - (a\cos^2\beta - 1/\rho) + (\sin\alpha\cos\beta - \sin\gamma)/R + F_2/R, \tag{c}$$

$$F_{12} = a_1'/R + a\sin\alpha\sin\beta\cos\beta - \sin\beta/R - F_1/R, \tag{d}$$

$$F_{22} = a_2 - a(1 - \sin^2\alpha\cos^2\beta) + \cos^2\gamma/\rho, \tag{e}$$

$$F_{111} = a_0'''/R^3 + 3a^2\sin\beta\cos^2\beta - 3a\sin\alpha\sin\beta\cos\beta/R + \sin\beta/R^2 + 3F_{12}/R + F_1/R^2, \tag{f}$$

$$F_{112} = a_1''/R^2 - 2(a\cos^2\beta - 1/\rho)/R + [a(1 - \sin^2\alpha\cos^2\beta) - \cos^2\gamma/\rho]/R + (\sin\alpha\cos\beta - \sin\gamma)/R - [a^2\sin\alpha\cos\beta(3\sin^2\beta - 1) + \sin\gamma/\rho^2] + (F_{22} - 2F_{11})/R + F_2/R^2, \tag{g}$$

$$F_{122} = a_2'/R + 2a\sin\alpha\sin\beta\cos\beta/R - a^2\sin\beta(3\sin^2\alpha\cos^2\beta - 1) - 2F_{12}/R, \tag{h}$$

$$F_{222} = a_3 - 3a^2\sin\alpha\cos\beta(\sin^2\alpha\cos^2\beta - 1) - 3\sin\gamma\cos^2\gamma/\rho^2, \tag{i}$$

$$F_{1111} = a_0''''/R^4 + \ldots. \tag{k}$$

$$F_{2222} = a_4 + 3\,a^3\,[1 - 6\sin^2\alpha\cos^2\beta + 5\sin^4\alpha\cos^4\beta) \qquad o)$$
$$- 3\,(1 - 6\sin^2\gamma + 5\sin^4\gamma)/\rho^3,$$

where $a_k = a_k(\phi)$ and $a_k'(\phi) = da_k/d\phi$, etc. The parameters $\alpha(\beta)$ and $a(\beta)$ of the outgoing spherical wave are given by the scan geometry [$\alpha = \alpha_c$, $a(\beta) = -\cos\beta/f$]. The relation $\beta(\phi)$ between the readout position ϕ and the deflection angle β is still unknown, but it will be determined later by the requirements of the scan [see also scan equation Eq.(3.21)]. The errors become finally also functions of the position ϕ, namely $F_{i..j} = F_{i..j}(\beta(\phi))$.

Now, step by step, we try to determine the coefficients $a_k(\phi)$ from Eqs.(5.18), while setting the errors $F_{i..j}$ to zero whenever possible. To obtain the functions $a_0'(\phi)$ and $a_1(\phi)$, we can set $F_1 = 0$ in Eq.(5.18a) and $F_2 = 0$ in Eq.(5.18b) without any restrictions and for any $\beta(\phi)$. When setting $F_{11} = 0$, an additional equation for $a_0(\phi)$ is obtained from Eq.(5.18c), which contains $a_0''(\phi)$. Since the relation $d(a_0')/d\phi = a_0''$ has to be fulfilled, we obtain now the scan equation [Eq.(3.21)], which determines the function $\beta(\phi)$. At this point, we have $F_1 = F_2 = F_{11} = 0$ realized and $\beta(\phi)$, $a_0(\phi)$, $a_1(\phi)$ determined.

Therefore, the error F_{12} in Eq.(5.18d) is completely determined and cannot be set to zero, unless an additional degree of freedom is introduced. As found in section 3.2 for the astigmatism, it is not possible to compensate for the error F_{12} when the scanning is constrained to a straight line ($\alpha = \alpha_c$). Only by accepting a curved scan line $\alpha(\phi)$ it is possible to set $F_{12} = 0$. Equation (5.18d) then determines the required deviation $\Delta\alpha(\phi) = \alpha(\phi) - \alpha_c$ [see Eqs.(3.29) and (3.30) in section 3.2.3].

The structure of the remaining equations (5.18e) through (5.18o) shows, that only the errors F_{22}, F_{222} and F_{2222} can be set to zero by choosing the functions $a_2(\phi)$, $a_3(\phi)$, and $a_4(\phi)$ appropriately, whereas all other $F_{i...j}$ are entirely given by the previously determined $a_k(\phi)$ and their derivatives. Note, that $F_{22} = 0$ determines an optimum solution for $a_2(\phi)$, but it does not necessarily correspond to an optimized astigmatism.

The analytical method reported in the preceding chapters requires, that for all scan positions the outgoing beam is focussed on the generated scan line $\mathbf{y}(t)$ with a minimum of astigmatism. If the geometry of the scan configuration and the scan line $\mathbf{y}(t)$ is specified, then the solution is already determined up to second order, and with it most of the higher order aberrations, which cannot be compensated by higher order terms in $\Phi(x,y)$. In particular, the coefficient a_0 determines the phase function on the line $\mathbf{x}(s)$ [$\Phi(\mathbf{x}(s)) = k\, a_0$] and the scan equation Eq.(3.21), describing the relation $\beta(\phi)$. Higher order corrections are essentially limited to the direction perpendicular to the scan line $\mathbf{x}(s)$. But they cannot compensate for the errors on the scan line, that are introduced by the second order theory.

Setting whenever possible the errors $F_{I,j}$ to zero is a straightforward analytical method. Such a procedure would yield phase functions $\Phi(x,y)$ for which the holographic scanners will have low aberrations and distortions. However, the optimum solution may correspond to a more balanced distribution of the errors $F_{I,J}$. This can be done, for example, by using numerical methods, which are beyond the scope of this thesis.

5.4 Design examples

To show the influence of higher order terms on the hologram phase function Φ, we shall present two typical design examples for disk configuration scanners. In each example one scanner was designed with a phase function up to second order, and another with a phase function up to fourth order. The analysis in these examples exploited the ray tracing method. Because the second order theory is more tractable, we found it useful first to optimize the phase function with respect to scan line geometry, focussing and astigmatism, in order to obtain the coefficients a_0, a_1 and a_2. Then, the coefficients a_3, a_4 can be determined from Eqs.(5.16i) and (5.16o) by setting $F_{222} = 0$ and $F_{2222} = 0$.

Case I

In the first example, the proposed design procedure is applied to a disk configuration scanner, that generates a straight line $\mathbf{y}(t)$ in space [$\alpha(\phi)$ = const].

The relevant parameters that were chosen are: the radius of the disk scanner R = 40 mm, the distance from the hologram to the scan line f = 300 mm, the beam diameter D = 5 mm and the maximum scan length L = ±105 mm. The incident wave was a divergent spherical wave with radius ρ = 610 mm, and the inclination angles of the outgoing and incident waves were α = 75 deg and γ = 0 deg, respectively.

Figure 5.1 shows the calculated spot diagrams at three different rotation positions ϕ_R of the holographic scanner, namely ϕ_R = 0, 8.3, 16.6 deg, which correspond to β = 0, 9.7, 19.3 deg, respectively. These are given both for the phase functions described up to second order (Fig.5.1a) as well as up to fourth order (Fig.5.1b). As shown, the hologram designed according to the second order approximation yields relatively poor spot quality. We determined, that this results from excessive aberrations when the phase function [in the direction perpendicular to the scan line $\mathbf{x}(s)$] is limited up to second order.

As shown in Fig.5.2b, such aberrations can be corrected by extending the phase function up to fourth order. For example, for ϕ_R = 16.6 deg, β = 19.3 deg, the standard deviation of the spot size for the second order solution is 107 µm whereas for the fourth order solution it reduces to 22 µm. Note, that the diffraction limited spot size is 38 µm (half intensity).

Case II

In the second example the design procedure was applied to a disk configuration scanner, which accepts a slightly curved scan line to compensate for the astigmatism of the outgoing wave, i.e. $\alpha = \alpha(\phi)$. This is the same scanner that was described in section 3.2.3. The incident beam was a plane wave ($\rho = \infty$) and the angles were $\alpha_C = -\gamma = 44.6$ deg. Furthermore, the disk radius was R = 40 mm, the distance from the hologram to the scan line f = 300 mm, the beam diameter D = 5 mm and the maximum scan length in the image plane L = ±105 mm.

Figure 5.2 shows the calculated spot diagrams at three different rotation positions ϕ_R of the holographic scanner, namely ϕ_R = 0, 6.2, 12.5 deg, which correspond to β = 0, 9.6, 19.3 deg, respectively. The spot diagrams of the scanners designed according to the second order approximation (Fig.5.2a) and

according to the fourth order approximation (Fig.5.2b) are nearly identical. So we see, that design procedures with higher order approximations do not always lead to improved results. In fact, for the configuration of case II, it is the second order approximation which already sets the lower limit on the spot size. It may be possible, however, to obtain more symmetric spots by additional manipulations of the errors $F_{l...j}$.

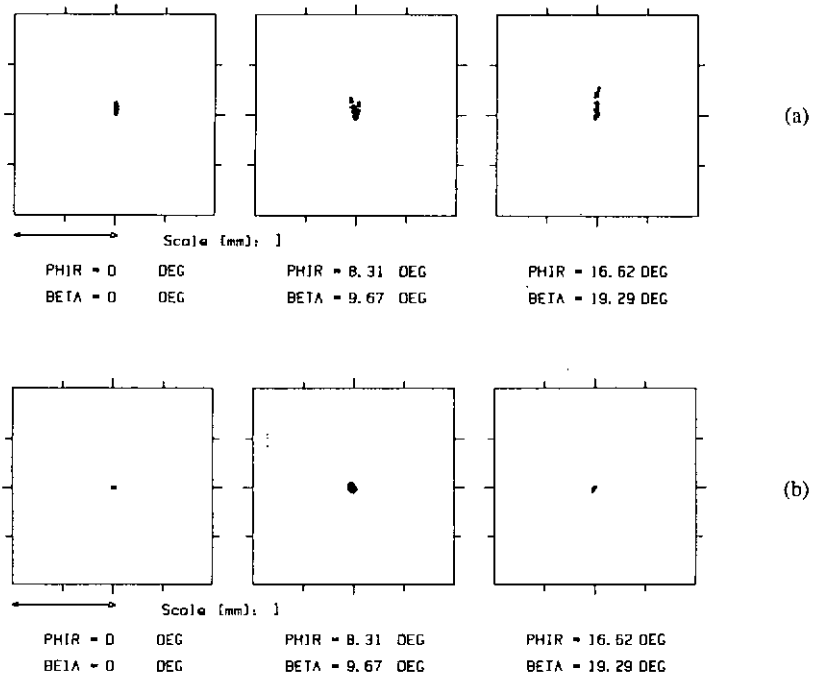

Figs.5.1. Spot diagrams for three circular positions ϕ_R (PHIR) of the hologram, corresponding to the scan angles β. The geometrical parameters (Fig.3.3) are f = 300 mm, D = 5 mm, R = 40 mm, the incident wave is a divergent spherical wave with ρ = 610 mm and the angles are $\alpha = 75$ deg, $\gamma = 0$ deg.
(a) Second order solution.
(b) Fourth order solution.

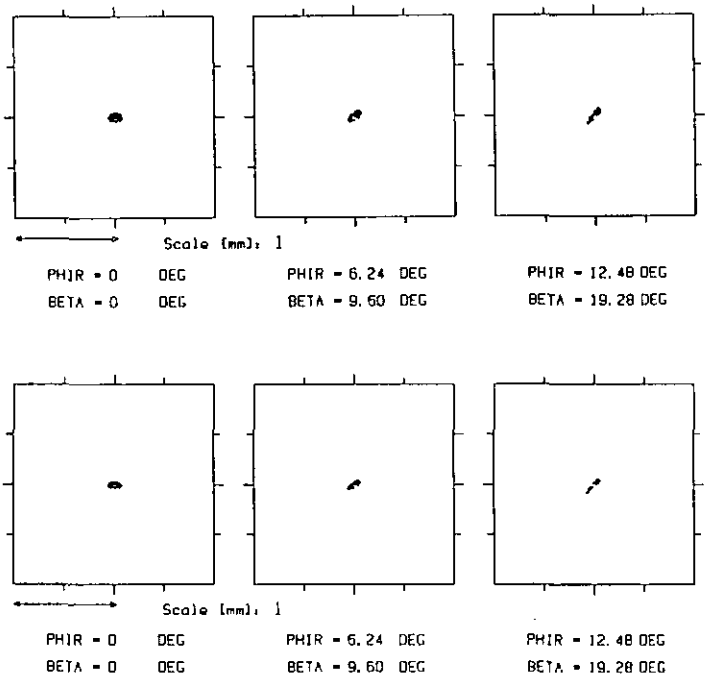

Figs.5.2. Spot diagrams for three circular positions ϕ_R (PHIR) of the hologram, corresponding to the scan angles β. The geometrical parameters (Fig.3.3) are f = 300 mm, D = 5 mm, R = 40 mm, the incident wave is a plane wave with $\rho = \infty$ and the angles are $\alpha = -\gamma = 44.6$ deg.

(a) Second order solution.

(b) Fourth order solution.

6. CONCLUSIONS

In the course of this research work we investigated a new analytical method for designing holographic disk scanners that generate straight lines $\mathbf{y}(t)$ in space. The results revealed, that in the direction of the scan line $\mathbf{x}(s)$ the solutions are completely determined by the first and second order derivatives, describing the direction and the curvature of the outgoing wave. Furthermore, we found that a circular motion cannot generate a straight line in space without astigmatism in the focal spot. By accepting a slightly curved scan line, the astigmatism can be eliminated and the spot quality improved.

The second order analytical solutions were examined with the help of geometrical ray tracing and compared with experimental results. We measured spot diameters (at half intensity) of less than 60 µm for a maximum scan line deviation of ±30 µm and less than 85 µm for a maximum scan line deviation of ±8 µm, for any position within the scan length of ±105 mm at an image plane distance of 300 mm. The experimental results and the theoretical predictions were in a good agreement.

Extending the method to higher order approximations, we found that aberrations perpendicular to the scan line can be minimized with appropriate corrections of the hologram phase function. However, astigmatism and other higher order aberrations, especially in the scan direction, cannot be removed completely. It is possible that numerical optimum design methods could be used to further improve the solutions found by our analytical approach.

Our design method needs not be restricted to holographic optical scanning elements. For example, other HOEs which have to transform a continuous set of input wavefronts into a continuous set of output wavefronts, can also be designed with our method.

ACKNOWLEDGMENTS

I wish to thank:

- Prof. R. Dändliker, director of this thesis, for his constant encouragement and his great knowledge from which I did benefit during many interesting discussions. I have truly enjoyed to work with him.

- Dr. H. Buczek, for the fruitful collaboration during the last years and for his helpful advices along the way.

- Prof. A. A. Friesem from the Weizmann Institute of Science, Rehovot, Isreal, for many discussions and for his help in editing this thesis.

- Prof. P. Martinoli for the interest he expressed in critically reviewing my thesis as member of the jury.

- All my family, friends, colleagues, the technical assistants and the secretarial staff of the Institut de Microtechnique, who made it possible to realize this work in a pleasant atmosphere.

This research was performed in close collaboration with the Optical Systems Department (Dr. Buczek, head) of the FSRM (Fondation suisse pour la recherche en microtechnique)/ CSEM (Centre suisse d'électronique et de microtechnique S.A.), Neuchâtel, where also the CGHs were produced. The research project was supported by the CERS (Comission pour l'encouragement de la recherche scientifique).

APPENDIX: Ray tracing

The performance of HOEs can be analyzed using the ray tracing method [27,28,29], which is very common in conventional lens design. In ray tracing through lens systems, the path of the light is determined with the help of elementary geometry, by successive application of the law of refraction (or reflection). In holography, the law of refraction has to be replaced by the law of grating diffraction.

The holographic recording and reconstruction process is essentially governed by the condition of phase matching in the hologram plane $\mathbf{x}_H = (x,y)$, which is given by

$$\Phi_P(\mathbf{x}_H) = \Phi_r(\mathbf{x}_H) + m\,[\Phi_O(\mathbf{x}_H) - \Phi_R(\mathbf{x}_H)] = \Phi_r(\mathbf{x}_H) + m\,\Phi_H(\mathbf{x}_H), \qquad (A1)$$

where the index P denotes the reconstructed wave front, r the reconstructing reference, O the object wave and R the recording reference wave. The hologram phase function is described by Φ_H; and the order of diffraction is indicated by m ($m = 0, \pm1, \pm2, \ldots$). Note, that in our case only the order +1 is of interest.

The phase matching condition [Eq.(A1)] in the hologram plane yields relations for the normal projections $\mathbf{k}_{iH}$ of the wavevectors $\mathbf{k}_i$ (i = P,r,O,R) onto that plane, namely

$$\mathbf{k}_{PH} = \mathbf{k}_{rH} + m\,[\mathbf{k}_{OH} - \mathbf{k}_{RH}] = \mathbf{k}_{rH} + m\,\mathbf{K}_H\,, \qquad (A2)$$

where the phase Φ and the wavevector $\mathbf{k}$ are related by $\mathbf{k}(\mathbf{x}_H) = \mathrm{grad}[\Phi(\mathbf{x}_H)]$.

The length of the wavevector during reconstruction is given by $|\mathbf{k}_r| = 2\pi/\lambda_r$. Thus for the component normal to the hologram plane the z-component k_{Pz} of the outgoing wave follows for a transmission HOE

$$k_{Pz} = \mathrm{sign}(k_r)\,[k_r^2 - \mathbf{k}_{PH}\,\mathbf{k}_{PH}]^{1/2} \qquad (A3)$$

$\mathrm{sign}(k_{Pz})$ denotes the sign of k_{Pz}. In the case of a reflection hologram, we have to write $-\,\mathrm{sign}(k_{Pz})$ in Eq.(A3).

Equations (A2) and(A3) describe the law of grating diffraction, which allows for tracing a finite ray through the holographic components.

The shape and the size of an image spot can be determined, by executing the ray tracing for a bundle of rays representing the illumination by a finite wavefront. In this thesis, the results are presented as spot diagrams (i.e. Fig.3.2), which are the points of intersection of the calculated rays with the image plane.

The propagation of the phase function can also be calculated with the aid of geometrical ray tracing, taking into account the optical path length. If the phase Φ_A is known at a point A, the phase Φ_B at another point B is given by

$$\Phi_B = \Phi_A + l\, n\, k, \qquad \text{(A4)}$$

where n is the refractive index and l the geometrical path length between the two points A and B.

REFERENCES

[1] L. D. Dickson, G. T. Sincerbox, A. D. Wolfheimer, "Holography in the IBM 3687 supermarket scanner", IBM J. Res. Dev. **26**, 228-234 (1982).

[2] H. Ikeda, M. Ando, T. Inagaki, "Aberration corrections for a POS hologram scanner", Appl. Opt. **18**, 2166-2170 (1979).

[3] H. Funato, "Holographic scanner for laser printer", Proc. Soc. Photo. -Opt. Instrum. Eng. **390**, 174-182 (1983).

[4] L. Beiser, "Imaging with laser scanners", Optics News, Nov. 1986, p. 10-16.

[5] Y. Ono, N. Nishida, "Holographic laser scanners for multidirectional scanning", Appl. Opt. **22**, 2128-2131 (1983).

[6] G. T. Sincerbox, "Holographic scanners: Applications, performance and design", in Optical Engineering, vol.8, "Laser beam scanning", G. F. Marshall, ed., (Marcel Dekker Inc. New York, 1985), p. 1-62.

[7] I. Cindrich, "Image scanning by rotation of a hologram", Appl. Opt. 6, 1531-1534 (1967).

[8] R. V. Pole, H. P. Wollenmann, "Holographic laser beam deflector", Appl. Opt. **14**, 976-980 (1975).

[9] L. Beiser, E. Darcey, D. Kleinschmitt, "Holofacet™ laser scanning-- an advanced data and image scanning technique", Proc. 1973 Electro-Opt. Syst. Des. Conf., p. 75.

[10] C. S. Ih, "Holographic laser beam scanners utilizing an auxiliary reflector", Appl. Opt. **16**, 2137-2146 (1977).

[11] C. Kramer, "Holographic laser scanners for nonimpact printing", Laser Focus, June 1981, p. 70 - 82.

[12] Y. Ono, N. Nishida, "Holographic laser scanners using generalized zone plates", Appl. Opt. **21**, 4542-4548 (1982).

[13] M. Malin, H. E. Morrow, "Wavelength scaling holographic elements", Opt. Eng. **20**, 756-758 (1981).

[14] W. H. Lee, "Computer-generated holograms: Techniques and Applications", in Progress in Optics, vol.16, ed. E. Wolf (North-Holland, 1978), p. 119-232.

[15] O. Bryngdahl, W. H. Lee, "Laser beam scanning using computer-generated holograms", Appl. Opt. **15**, 183-194 (1976).

[16] H. Iwaoka, T. Shiozawa, "Aberration-free linear holographic scanner and its application to a diode-laser printer", Appl. Opt. **25**, 123-129 (1986).

[17] Y. Ono, N. Nishida, "Holographic optical elements with optimized phase-transfer functions", J. Opt. Soc. Am. A **3**, 139-142 (1986).

[18] K. A. Winick, J. R. Fienup, "Optimum holographic elements recorded with nonspherical wave fronts", J. Opt. Soc. Am. **73**, 208- 217 (1983).

[19] J. Kedmi and A. A. Friesem, "Optimized holographic optical elements", J. Opt. Soc. Am. A **3**, 2011-2018 (1986).

[20] H. P. Herzig, R. Dändliker, "Holographic optical scanning elements: Analytical method for determining the phase function", J. Opt. Soc. Am. A **4**, 1063-1070 (1987).

[21] H. P. Herzig, R. Dändliker, "Design rules for holographic optical scanning elements", Fourth International Symposium on Optical and Optoelectronic Applied Science and Engineering, The Hague 1987, to be published in Proc. SPIE **812**.

[22] R. Dändliker, K. Hess, T. Sidler, "Astigmatic pencils of rays reconstructed from holograms", Israel J.Technol. **18**, 240-246 (1980).

[23] H. P. Herzig, "Holographic optical elements (HOE) for semiconductor lasers", Opt. Commun. **58**, 144-148 (1986).

[24] H. Kogelnik, "Coupled wave theory for thick hologram gratings", Bell. Syst. Tech. J. **48**, 2909-2947 (1969).

[25] B. R. Brown, A. W. Lohmann, "Complex spatial filtering with binary masks", Appl. Opt. **5**, 967-969 (1966).

[26] M. Born, E. Wolf, "Principles of optics", (Pergamon Press, Oxford, 1980).

[27] J. N. Latta, "Comuter-based analysis of holography using ray tracing", Appl. Opt. **10**, 2698-2710 (1971).

[28] W. T. Welford, "A vector raytracing equation for hologram lenses of arbitrary shape", Opt. Commun. **14**, 322-323 (1975).

[29] W. T. Welford, "Aberrations of optical systems", (Adam Hilger Ltd, Bristol, 1986).